PREVENTION OF CALCIUM SULPHATE CRYSTALLISATION IN WATER DESALINATION PLANTS USING SLURRY PRECIPITATION AND RECYCLE REVERSE OSMOSIS (SPARRO)

A Lewis • J Nathoo

WRC Report No. 1372/1/06

Water Research Commission

PREVENTION OF CALCIUM SULPHATE CRYSTALLISATION IN WATER DESALINATION PLANTS USING SLURRY PRECIPITATION AND RECYCLE REVERSE OSMOSIS (SPARRO)

Report to the
WATER RESEARCH COMMISSION

By

Alison Lewis and Jeeten Nathoo

Precipitation and Crystallisation Research Facility
Department of Chemical Engineering
University of Cape Town

WRC Report No 1372/1/06
ISBN No 1-77005-383-2

FEBRUARY 2006

Disclaimer

This report emanates from a project financed by the Water Research Commission (WRC) and is approved for publication. Approval does not signify that the contents necessarily reflect the views and policies of the WRC or the members of the project steering committee, nor does mention of trade names or commercial products constitute endorsement or recommendation for use.

Printed by Silowa Printers 012 804 1164

EXECUTIVE SUMMARY

BACKGROUND

The principal objective of the research project was to investigate the Slurry Precipitation and Recycle Reverse Osmosis (SPARRO) process from a crystallisation perspective. To achieve this objective, the following aims were identified:

1. To expand both the fundamental and practical understanding of the operation of the Slurry Precipitation and Recycle Reverse Osmosis (SPARRO) system;
2. To develop design specifications relating to the crystallisation parameters of the system and the control of the desupersaturation reactor based on the critical operating parameters for the SPARRO system;
3. To develop design specifications relating to membrane selection and treatment in the SPARRO system;
4. To define the critical operating parameters for the SPARRO system.

OVERVIEW

Tasks relating to the crystallisation aspects of the project are complete and considerable success has been achieved in this area. Detailed information can be found in the MSc thesis of Shilpa Seewoo (Seewoo, 2003). Tasks relating to the membrane aspects of the project are also complete. Two dedicated process systems and associated equipment have been designed and commissioned during the course of this project: the Sparro Membrane Test Rig (SMTR) mini-plant and the Directed Slurry Spraying Technique (DSST).

Considerable progress has been made in addressing the central question of this research project, which is: **To what extent do the crystallisation parameters affect membrane damage in the SPARRO system?**

Aim 1: To expand both the fundamental and practical understanding of the operation of the Slurry Precipitation and Recycle Reverse Osmosis (SPARRO) system

Fundamental and practical understanding of the SPARRO system has been expanded through the literature review and the experimental program, as well as through interaction with industrial partners in the project. These aspects are presented in more detail in the body of the report.

Aim 2: To develop design specifications relating to the crystallisation parameters of the system and the control of the desupersaturation reactor based on the critical operating parameters for the SPARRO system;

The crystallisation aspects of the process have been thoroughly investigated and an extensive understanding of gypsum crystal behaviour developed. Design specifications relating to the crystallisation parameters of the system and control of the desupersaturation reactor have been developed based on the critical operating parameters for the SPARRO system.

The conclusions from the crystallisation aspects of the work are as follows:

- Rate of consumption of supersaturation is significantly increased by the use of seeds as a source of secondary nucleation;

- Needle-like seeds were produced under conditions of low supersaturation and were characterised by a long induction time;
- Plate-like seeds were formed at high supersaturation, with a significantly reduced induction period;
- Digital image processing could be used to quantitatively distinguish between gypsum morphologies;
- XRD analysis showed similar traces for all morphologies and analytical grade gypsum;
- Sulphate to calcium ratio and pH extremes affected the solubility of gypsum and thus the rate of desupersaturation by the common ion effect and influence on the speciation of SO_4^{2-} and Ca^{2+};
- Seed morphology controlled the morphology at equilibrium under the batch conditions investigated;
- At low seed concentrations, the plate-like seeds significantly reduced desupersaturation times due to higher specific surface area;
- The kinetic rate constant for growth was affected by seed quantity (due to available surface area);
- Increased agitation reduced desupersaturation time and relative increase of seed size, suggesting attrition under conditions of high turbulence;
- Statistical analysis confirmed that, of the four factors tested, the seed quantity had the most significant effect on all three response variables;
- A set of operating conditions were identified to minimise desupersaturation time, while still maintaining a plate-like precipitate morphology

Aim 3: To develop design specifications relating to membrane selection and treatment in the SPARRO system;

The following progress has been achieved with this task:

In the early stages of the project, it was established that the only locally manufactured membranes are cellulose acetate (CA) and thus it was decided to restrict the membrane investigation to these.

A single membrane module, the SPARRO Membrane Test Rig (SMTR) through which feed slurry with specific crystal characteristics is recycled in a closed loop circuit under specified operating conditions was constructed. Commissioning problems and difficulties in inflicting significant membrane damage hampered progress in membrane testing with the SMTR. Modifications to the test work included operating the system at the highest possible linear velocity (2.44m/s) and with an increased concentration of gypsum crystals in the feed. Based on this method of experimentation, the following conclusions can be drawn:

- For intermittent SMTR operation over a total operational time of 200 hours, the needle type morphology had a greater detrimental effect on both salt rejection and membrane flux, with the system taking up to 8 hours to return to the optimal performance levels subsequent to a shut down.
- For continuous SMTR operation with a seeds concentration of 2.14g/L, over a total operational time of 160 hours, it is evident that the needle morphology shows a greater degree of variability in salt rejection and membrane flux when compared to the platelets.
- For continuous operation, with a seeds concentration of 14g/L, over an operational time of 180 hours, there was no significant variation in the salt rejection over time, when compared

to the results of the standard salt test, which would be indicative of membrane damage having occurred for either a needle or platelet type morphology.

The following conclusions can be drawn with regards to the experimentation using the novel Directed Slurry Spraying Technique (DSST) that was developed during the course of the project:

- It is clear that, for both morphologies, the extent of damage due to scouring is significantly less at a spraying angle of 45°, which would be more representative of the angle of impact of the crystals with the surface in normal operational mode.
- When comparing the membrane surfaces that were sprayed with the two different morphologies, the damage caused by the needle type morphology was significantly more pronounced than that of the platelet type morphology. This compliments the results obtained using the SMTR by demonstrating that the crystal morphology does have the potential to play a significant role in membrane damage. Conclusive evidence was generated that the needle type morphology has a significant impact on membrane damage compared to the platelet type morphology under these testing conditions.
- The implications of this work are that, if the platelet morphology of the crystals in the SPARRO process is maintained, membrane damage is expected to be reduced.

Based on the DSST experimental work that has been carried out, it is apparent that, although there is evidence that gypsum crystal morphology of a needle type does have the potential to influence membrane damage through scouring, under typical SPARRO operating conditions, simulated by the SMTR-mini plant, the evidence that the different morphologies actually damage the membranes is inconclusive. This therefore shifts the focus onto membrane fouling as the predominant membrane damaging mechanism and as the reason for the failure in the SPARRO process.

Aim 4: To define the critical operating parameters for the SPARRO system.

This aim depended on the crystallisation and membrane aspects of the work being integrated and was addressed in the latter stages of the project.

Aqueous chemistry modelling was carried out using predictive thermodynamic software in order to ascertain how the complex aqueous chemistry of the real waters under consideration would affect the findings of this research which, of necessity, is based on synthetic waters. It was found that:

- For the selected mine waters, a water recovery of approximately 60% is achievable before the supersaturation increases to the scaling level. The Grootvlei phase 1 and phase 2 waters are both supersaturated with respect to $Al(OH)_3$ which is responsible for the fouling mentioned in Juby's (Juby, 1994) report. The Grootvlei phase 2 water is also supersaturated with respect to $CaSO_4.2H_2O$;

The implications of the two modelling exercises for the complex mine waters under consideration are contradictory:

- On the basis of water composition, the scaling potential of the complex mine waters is increased compared to the pure solution;
- On the basis of ionic strength, the scaling potential of the complex mine waters is decreased compared to the pure solution;

More detailed modelling and experimental studies would need to be carried out in order to establish the net result of these two counteractive effects.

Based on the findings of the membrane aspects of the research, it is clear that membrane fouling as a result of the feed being supersaturated with respect to Al(OH), was the predominant cause for membrane failure in the SPARRO process. However, whilst the evidence is inconclusive with regards to crystal morphology categorically causing membrane damage, there is evidence of morphology having an influence on membrane performance. Consequently, from the SPARRO Membrane Test Rig (SMTR) mini-plant studies and the Directed Slurry Spraying Technique (DSST), it is clear that, besides aqueous chemistry, control of crystal morphology is essential in order to minimise membrane damage in the SPARRO process. In this process there are three parameters that can be used to control morphology:

- Supersaturation to control nucleation
- Supersaturation to control growth
- Seed volume to control morphology

- If heterogeneous nucleation in the membrane is to be avoided, the supersaturation must be controlled. This can be manipulated by adjusting the water recovery.
- If sufficient seeds are provided, the morphology of the gypsum crystals can be controlled to the platelet shape, **even in regions where the needle morphology is dominant**. Thus, the membrane damaging needle-like morphology can be avoided.

Model design charts that relate seed volume and supersaturation or sulphate: calcium ratio to gypsum morphology in pure solutions have been developed.

RECOMMENDATIONS

The major recommendation arising from this work is related to the level of understanding of the chemistry of the mine waters being treated using the SPARRO process. It is recommended that full analyses should always be carried out on waters of interest.

It is also recommended that future work focus on the aqueous chemistry of real mine waters, and the implications of that aqueous chemistry for interactions in the aqueous phase as well as for scaling species.

ACKNOWLEDGEMENTS

The writers wish to express their gratitude:

- To the staff of the Crystallisation and Precipitation Research Facility and the Mechanical Workshop, both of the Chemical Engineering Department at the University of Cape Town for their contribution to the research reported here and;
- To Bernard Canon and Weir-Envig for the generous supply of membranes necessary for the testing;
- To the members of the Water Research Commission (WRC) Steering Committee who guided the research work and provided invaluable help during the research period:

  Dr G Offringa – WRC
  Mr Pieter Smit - Co-ordinator WRC
  Mr O Hempel – Committee Secretary WRC
  Dr J Smit – Anglo American Research Laboratories
  Mr Doep du Plessis and Deon Nieuwenhuys – Sasol Technology,
  Prof EP Jacobs – Institute for Polymer Science, University of Stellenbosch
  Prof C Buckley – Pollution Research Group, University of Natal

OUTPUTS AND CAPACITY BUILDING

OUTPUTS

Specific outputs from the project include:
3 BSc (Chem Eng) currently registered;
1 BSc (Chem Eng) Honours project research thesis;
1 MSc (Chem Eng) research thesis;
1 international conference presentation;
6 local conference presentations.
1 journal paper in an internationally refereed journal
1 journal paper in prep.
1 keynote address at a local conference.

CAPACITY BUILDING

The Department of Chemical Engineering has a comprehensive programme for the training and education of engineers at both the undergraduate and postgraduate level. The department has an undergraduate student body of approximately 300 students, graduating on average 55 students per year of whom two thirds are Black and one third women. The postgraduate student body has approximately 120 students of which 32% are Black and 29% women.

Within this student group, this WRC project has provided the opportunity for the training of three Post Doctoral Fellows and two MSc students over its three year duration. Of these, three were Black and two female. In addition, it has provided five undergraduate and Honours level students with opportunity for exposure to research. During the project, Jeeten Nathoo, who first became involved as an undergraduate student, advanced to the extent that he is now employed as a full time research officer in the Precipitation and Crystallisation Research Facility.

Students and staff involved in the project include:

1. Thembinkosi Magubane (South African, African male)
   BSc (Chem Eng) 3rd year (2004)
2. Yu Lun Chiang (South African, Asian male)
   BSc (Chem Eng) 3rd year (2005)
3. Majoang Makhosi (South African, African male)
   BSc (Chem Eng) 3rd year (2005)
4. Bonginkosi Mgweba (South African, African male)
   BSc (Chem Eng) 3rd year (2005)
5. Oliver Zeitler (German Intern Student) (German, white male)
   Diploma Ingenieur (Chemical) 3rd year (2005)
6. Jeeten Nathoo (Zimbabwean, Indian male)
   BSc (Chem Eng) Hons research project (2001)
   MSc Chem Eng research project (2002 and 2003)
7. Shilpa Seewoo (Mauritian, Indian female)
   BSc (Chem Eng) Hons research project (2001)
   MSc Chem Eng research project (2002 and 2003)

8. Rob van Hille (South African, white male)
   Post doctoral research fellow (2002 and 2003)
9. Yi Fei Zhang (Chinese, male)
   Post doctoral research fellow (2004 and 2005)

PUBLICATIONS

1. Lewis, A.E. and Nathoo, J., 2005. Scale prediction in real mine waters, *Mineral Processing 2005*, Cape Town, 4 -5 August 2005, OR33, p. 55
2. Lewis, A.E., 2005. Pitfalls in Real World Particle Characterisation, *7th International Conference on Crushing and Grinding*, Midrand, Gauteng, 23 February 2005. (Keynote address)
3. Zhang, Y., and Lewis, A.E., Real world complications in the measurement of particle size, *Mineral Processing 2004*, Cape Town, 4 - 6 August 2004, pp. 93
4. Seewoo, S., van Hille, R., and Lewis, A.E., 2004. Aspects of gypsum precipitation in scaling waters, *Hydrometallurgy*, 75, 135-146
5. Seewoo, S., van Hille, R. and Lewis, A.E., 2003. Control of the morphology of gypsum in the desupersaturation reactor used in the SPARRO process, *5th WISA-MTD Workshop: Membrane Developments in Waste Minimisation, Water Treatment and the Process Industry*, Vereeniging, 30 March – 2 April 2003.
6. Seewoo, S., Lewis, A.E., Lacour, S. and van Hille, R., 2002. Control of the desupersaturation reactor in the slurry precipitation recycle reverse osmosis (SPARRO) process, *Mineral Processing 2002*, Cape Town, 1-2 August 2002.
7. Seewoo, S., 2003. Morphology control in gypsum precipitation. MSc Thesis, University of Cape Town
8. Nathoo, J., van Hille, R. and Lewis, A.E., 2003. Investigating the effect of gypsum crystal morphology on membrane damage in the SPARRO process, *5th WISA-MTD* Workshop*: Membrane Developments in Waste Minimisation, Water Treatment and the Process Industry*, Vereeniging, 30 March – 2 April 2003.
9. Nathoo, J., Lewis, A.E., Lacour, S. and van Hille, R., 2002. Investigating the effect of gypsum crystal morphology on membrane damage in the SPARRO process, *Mineral Processing 2002*, Cape Town, 1-2 August 2002.
10. Nathoo, J. and Lewis, A.E., (In prep). An accelerated approach to determining the impact of gypsum morphology on membrane damage through scouring.
11. Nathoo, J and Seewoo, S., 2001. *The SPARRO process for desalination of calcium sulphate scaling waters*, BSc (Chem Eng) Research Project, Chemical Engineering Department, University of Cape Town (Final mark obtained: 79%)
12. Lewis, A.E., Nathoo, J., Seewoo, S. and Lacour, S., 2002. Prevention of scaling in mine waters using Slurry Precipitation and Recycle Reverse Osmosis (SPARRO), *15th Industrial Crystallisation Conference*, Sorrento, Italy, 15-18th September 2002.

TABLE OF CONTENTS

TABLE OF FIGURES

TABLE OF TABLES

1. INTRODUCTION

Ground water, particularly from South Africa's gold mining operations, has a high calcium sulphate scaling potential. It is estimated that on an annual basis, in the South Africa gold mining industry alone, poor mine service water costs the industry in the region of R300 million based on its corrosive, scaling and fouling potential (Mackay *et al.*, 1991). The oxidation of pyrite ores present in gold bearing reefs are responsible for introducing sulphate into the ground water and lowering its pH whilst the elevated calcium levels are as a result of the addition of lime during the neutralisation process (Juby, 1994). Recycling a major part of the water effluent stream further increases the concentration of these dissolved salts.

The Slurry Precipitation and Recycle Reverse Osmosis (SPARRO) process was developed in the early 1980's with the primary objective of desalinating water with a high calcium sulphate concentration efficiently and economically (Juby *et al.*, 1992). The process uses tubular cellulose acetate membranes in a seeded slurry system (Juby and Schutte, 2000) and has also been applied for the removal of heavy metals from aqueous waste (Sluys *et al.*, 2001) and to water softening (Verdoes and Hanemaaijer, 1994; 1996). Harries (1985) concluded that the tubular cellulose acetate (CA) membranes performed satisfactorily in the seeded slurry mode with no evidence of fouling, scaling or damage to the membranes. This was at seed slurry concentrations of approximately 40g/L. However, later research (Juby and Schutte, 2000; Busby *et al.*, 1991), reported problems with fouling, corrosion and hydrolysis (defined in the context of their research as membrane damage resulting in an increase in membrane flux together with a decrease in permeate salt rejection), point to the fact that many process and equipment related questions remain unanswered.

Research aimed to establish the cause of the problems in operating the SPARRO system and develop a greater understanding of the mechanisms at work. In particular, the involvement of expertise in the field of crystallisation and precipitation where this process is known as Membrane Assisted Crystallisation (MAC) (Kramer & Jansens, 2002) enabled the problem to be viewed from a hitherto unexamined angle. The main focus has been on the effect of gypsum, which has the highest dissolved salt concentration of scaling mine water. From literature (Christoffersen et al., 1982) and experimental investigation (Lewis et al., 2002), it has been established that, depending on the experimental conditions, gypsum occurs as two primary morphologies: needles and platelets as shown below in. Figure 1.

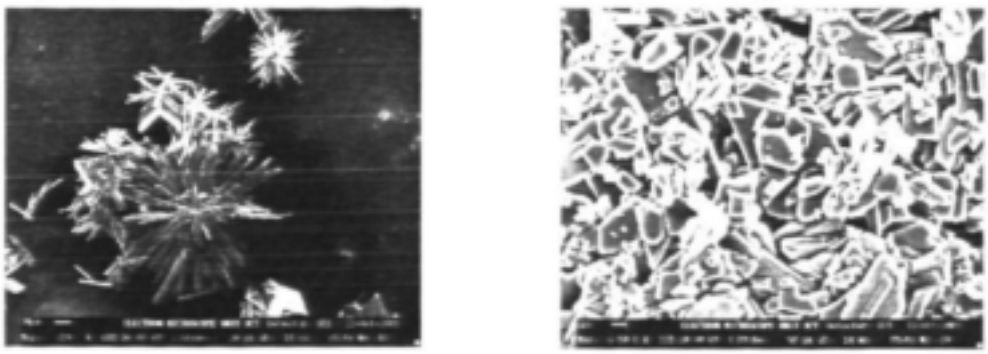

Figure 1: Gypsum crystals of needle (left) and plate (right) type morphology

In terms of comparing the relative hardnesses of the two types of gypsum morphologies as an indication of which of these two would be more likely to affect membrane damage, it was

established that there is an insignificant difference between the hardness values of the two morphologies. Gypsum is used as a reference in the Mohs Hardness Scale and has a value of 2 on a scale of 0 (chalk) to 10 (diamond).

The intention was to test specific gypsum crystal morphologies and different system operating conditions in the membrane process in order to relate membrane life expectancy to specific crystal characteristics. Once established, it was intended that this information be used to modify the SPARRO process operating conditions: in terms of membrane selection, seeding and control of the desupersaturation reactor to improve membrane performance and life expectancy.

It was initially proposed to revisit the problem using thin-film composite membranes, possible membrane pre-coating as a membrane protection mechanism and to investigate the effect of temperature adjustment on membrane performance and seeded crystal behaviour. However, given that the only locally manufactured membranes are cellulose acetate (CA) and thus it was decided to restrict the membrane investigation to these. Temperature adjustment was not considered to be feasible for the large volumes involved and this parameter was thus not investigated.

2. OBJECTIVES

a) To expand both the fundamental and practical understanding of the operation of the Slurry Precipitation and Recycle Reverse Osmosis (SPARRO) system;
b) To develop design specifications relating to the crystallisation parameters of the system and the control of the desupersaturation reactor based on the critical operating parameters for the SPARRO system;
c) To develop design specifications relating to membrane selection and treatment in the SPARRO system;
d) To define the critical operating parameters for the SPARRO system.

3. BACKGROUND

3.1. South African mine waters & scaling

Most South African gold mine service waters have high calcium and sulphate concentrations, the source of sulphate ions being oxidation of pyrite ores present in gold bearings. The presence of calcium is as a result of addition of lime to mine waters for neutralisation purposes. (Juby et al, 1985) Typical compositions and quality of mine waters are given in Table 1.

Table 1: Quality of mine service water from two different South African mines (Juby, 1994)

Determinant	Units	Orange Free State Mine	West Rand Mine
TDS (total dissolved solids)	Mg/L	3800	2200
pH		6.5	6.0
Sodium	mg Na/L	1000	170
Calcium	mg Ca/L	330	400
Sulphate	mg SO_4/L	1050	1400
Chloride	mg Cl/L	1400	60
Magnesium	mg Mg/L	30	50

From Table 1, it can be seen that these mine waters are dominated by the presence of calcium and sulphate. The degree of calcium sulphate saturation may have severe implications in desalination because of scaling (Juby, 1994) and there is scaling potential whenever the solubility of sparingly soluble salts, such as calcium sulphate, is exceeded (Juby and Schutte, 2000). Scale formation is a serious problem, since it is implicated in decline in volume capacity of equipment; blockage of pipes; corrosion and fatigue of metal parts and reduction in heat transfer rates (Sohnel and Garside, 1992). In addition, calcium sulphate also contributes to the environmental pollution load (Juby and Schutte, 2000).

3.2. SPARRO process review

The block flow diagram of the SPARRO process is shown in Figure 2

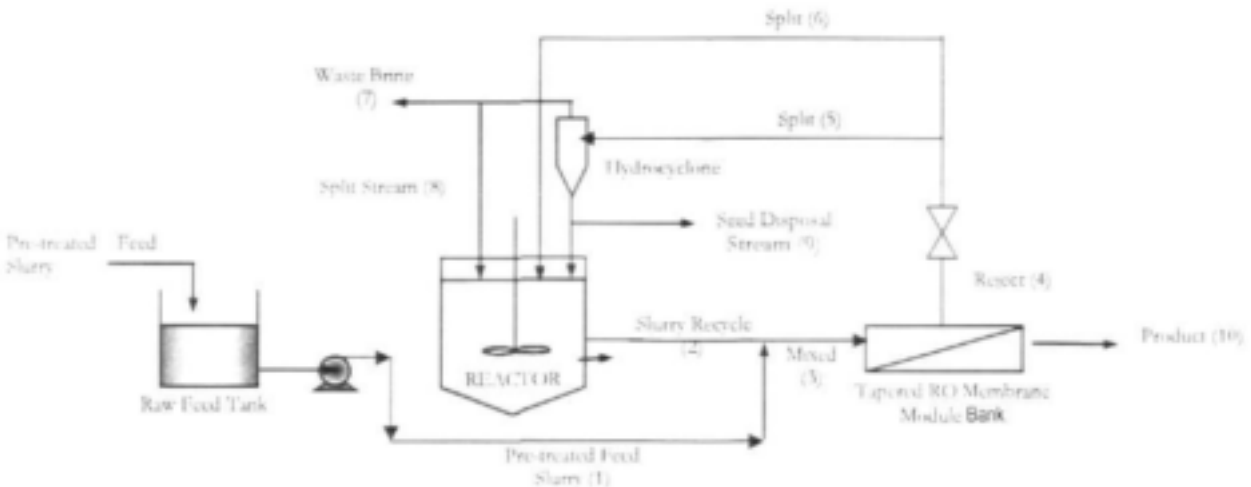

Figure 2: Block Flow Diagram of the SPARRO process (Juby, 1994)

Feed water is pre-treated by the removal of any undesirable material from the water to avoid degradation of the membranes. Conditioning of the water is also required so that it is suitable for the specific type of membrane used in the process. This involves the regulation of pH and temperature. The pre-treated and conditioned feed water is stored in a feed water tank and pumped to a gauge pressure of around 4000kPa. This pressurised raw feed water (stream 1) mixes with the gypsum slurry recycle (stream 2) at a specified mixing ratio. The

recycle slurry stream contains approx 41g/L of gypsum crystals in suspension whilst the mixed stream (stream 3) contains approx 18g/L of gypsum crystals in suspension.

Stream 3 is passed through the tapered membrane modules at a gauge pressure of 4000kPa and a total dissolved solids (TDS) concentration of 7500 mg/L.

The SPARRO process is based on Seeded Reverse Osmosis (SRO), which involves circulating the slurry of seed crystals within the reverse osmosis (RO) system. As the solubility product is exceeded because of the concentration effect, precipitation of the $CaSO_4$ is initiated. Instead of the $CaSO_4$ forming scale on the membrane, the seed crystals provide preferential growth sites for the $CaSO_4$ to grow, thus minimising the problems associated with membrane scaling. The membrane separates stream 3 into a purified effluent stream (permeate product) and a stream (reject) more concentrated in solute, the crystals that are too large to pass through the membrane pores.

The membrane reject (stream 4) is delivered at a pressure of 2500 kPa and has a TDS of approx 15 000 mg/L and 36.5g/L gypsum crystals in suspension. Concentration effects within the membranes are the cause of increase in the TDS. The pressure of the stream 4 is reduced to 510 kPa by passing it through a pressure reducing orifice plate. The stream is then split into a controlled volume (stream 5), which is sent to the hydrocyclone, and the remainder (stream 6) is sent to the reactor.

A controlled volume (stream 8) of the overflow of the hydrocyclone is returned directly to the reactor. The remainder, waste brine (stream 7), is disposed of. Seed blowdown (stream 9) is removed from the underflow while the bulk of the underflow of the hydrocyclone is sent to the reactor. Stream 9 maintains the required suspended solids concentration in the system.

In the reactor, mechanical stirring ensures complete mixing during the time required for desupersaturation of the supersaturated solutions, which return to the reactor from the membrane module. The product (stream 10) is the permeate from the membrane module and has a TDS of approx 900 mg/L.

* **SPARRO Process Operating Conditions**

Operating pressure:	4000kPa
Linear velocity through membrane:	$1.25ms^{-1}$

41g/L gypsum in slurry recycle stream
18g/L solids in stream entering membrane module
7500mg /L TDS in stream entering membrane module
900mg/L TDS in permeate from membrane modules

3.3. The desupersaturation reactor

The desupersaturation reactor acts as a storage buffer for the seed crystals that are required in the feed stream to the membranes. It provides sufficient residence time to allow the supersaturated brine solution that exits the membrane stack to return to equilibrium conditions. This is achieved by allowing the excess $CaSO_4$ to precipitate on the seed crystals present in the slurry. A mechanical stirrer ensures complete mixing during the time required

for desupersaturation of the supersaturated solutions that return to the reactor from the membrane. (Juby, 1994)

Juby (1994) designed the research reactor on the basis of results obtained from an investigation into the kinetics of gypsum carried out by Marce *et al* (1988). The design capacity of the SPARRO process was 0.82 l/s. Operating conditions were a slurry concentration in the reactor of 40g/L and an assumed approach to equilibrium of 95%. The residence time required to achieve 5 % of the equilibrium conditions was calculated to be 0.9 hours. The calculated reactor vessel volume was 2.4 m^3 and the operating capacity was set to 3.5 m^3 to avoid overflows. The specifications of the reactor designed by Juby (1994) follow in Table 2.

Table 2: SPARRO reactor design specifications (Juby, 1994)

Description	Value
Maximum capacity [m^3]	4.5
Design capacity [m^3]	3.5
Diameter [m]	1.5
Height [m]	2.5
Power [kW]	0.75
Speed [rpm]	290
Hydraulic residence time [h] (at design)	1

The reactor contents and the outlet stream had a solid suspension concentration of 41g/L. This means that the quantity of solids (gypsum) in solution amounts to 1.76% by volume.

4. Theory And Literature Review

4.1. Calcium Sulphate

Calcium Sulphate in natural deposits exists predominantly in the dihydrate ($CaSO_4.2H_2O$) form commonly referred to as gypsum. The anhydrite ($CaSO_4$) form is present to a lesser extent while the hemihydrate form ($CaSO_4.½H_2O$) is normally produced from the dihydrate form when it is heated to remove water.

Of these three forms, the dihydrate, also known as gypsum, is the compound that is of major interest as it is predominantly present at ambient conditions. Crystals of gypsum are apt to be curved or even lenticular. In twins this sometimes produces arrowhead forms (Miers, 1929). The structure of gypsum consists of strongly bonded layers of SO_4^{2-} and Ca^{2+} with alternating layers of H_2O. Hydrogen bonding holds the H_2O molecules to the $CaSO_4$ layers and allows for cleavage (Nesse, 2000).

Table 3: Physical properties of forms of calcium sulphate (Kirk Othmer,1995)

Property	Dihydrate, $CaSO_4.2H_2O$	Hemihydrate, $CaSO_4.0.5H_2O$	Anhydrite, $CaSO_4$
Molecular weight	172.17	145.15	136.14
Transition point, 0C	128[a]	163[b]	
Melting point 0C	1450[c]	1450[c]	1450[c]
Specific Gravity	2.32		2.96
Solubility at 25°C, g/100g H_2O	0.0151*		

a Hemihydrate form
b Anhydrous material is formed
c Compound decomposes
* Christoffersen *et al* (1982)

Christoffersen *et al* (1982) experimentally determined the solubility of gypsum. Some growth experiments were conducted in a closed system and continued until a constant concentration of calcium was measured by an EDTA titration method. The solubility limit obtained for gypsum was C_s=0.0151 ± 0.0001 M. This is in agreement with the solubility value of gypsum of 0.015M obtained experimentally by Lash *et al* (1984).

4.2. Gypsum Crystal Synthesis

Lash & Burns (1984) produced both needle and platelet gypsum ($CaSO_4.2H_2O$) crystals at room temperature by varying the initial reagent concentrations. The needle morphology was produced from solutions whose initial concentration was greater than 0.4M in $CaSO_4$ whilst the platelet morphology was produced from solutions whose initial $CaSO_4$ concentration was less than 0.25M. Conversely, Christoffersen *et al* (1982) found that low concentrations (0.3M $CaSO_4$) favoured the needle-like morphology, whereas high reagent concentrations (0.725M $CaSO_4$) produced smoother surfaces. Liu & Nancollas (1969) added seed crystals to stable supersaturated solutions and formed needle-like monoclinic crystals 80-120μm long in 0.1M gypsum solutions and 30-50μm long in 0.6M solutions.

4.3. Precipitation Theory

Supersaturation is the thermodynamic driving force for any precipitating process and is the key variable in setting the mechanisms and rates of the steps involved in precipitation (Mullin, 2001). Supersaturation, S, of a solution is given by the normalised difference between the concentration of the solution, C, and the solubility limit, C^*, as given in equation (1) (Sohnel & Garside, 1992) although a number of different definitions exist in the literature.

$$S = \frac{C - C^*}{C^*} \qquad (1)$$

Precipitation involves a number of primary kinetic processes such as nucleation and crystal growth and secondary processes such as ageing and agglomeration. (Sohnel & Garside, 1992)

Nucleation

The theoretical description of nucleation depends on the mechanism responsible for nucleus formation. Primary nucleation is the formation of a new solid particle in the absence of an existing nucleus of the solid phase. Two possible mechanisms can occur: homogeneous nucleation, which takes place when a nucleus forms without the presence of any solid phase and heterogeneous nucleation, which occurs when a nucleus is formed in the presence of a foreign solid phase. In secondary nucleation, it is the presence of the crystallising material that promotes the formation of a nucleus. (Sohnel & Garside, 1992)

Crystal growth

Crystal growth is the enlargement of crystals caused by the deposition of solid material onto a nucleus. Crystal growth rate is defined as the rate of displacement of a given crystal face in the direction perpendicular to the face. Crystal growth can be limited by:

- Transport from solution to the crystal surface by volume diffusion or convection or by both of these mechanisms;
- Incorporation of material into the crystal lattice through a surface integration process, which is more commonly referred to as a surface reaction. (Sohnel & Garside, 1992).

Secondary processes

Processes such as ageing and agglomeration cause further changes of the physical and chemical properties of the precipitated phase. Ageing is a slow process and involves a change in the solid phase, changes of the crystal modification, habit, specific surface or chemical composition of the solid phase. Agglomeration is the clustering of smaller particles to form a cemented aggregate of larger particles. (Sohnel & Garside, 1992)

Kinetics of precipitation

The individual steps and kinetic processes comprising precipitation are illustrated in Figure 3 (Sohnel & Garside, 1992). The time scale over which precipitation takes place can vary from a few seconds to a number of days. Supersaturation is the key variable in any precipitation, the level of supersaturation in the precipitating solution governing the rates of the various processes.

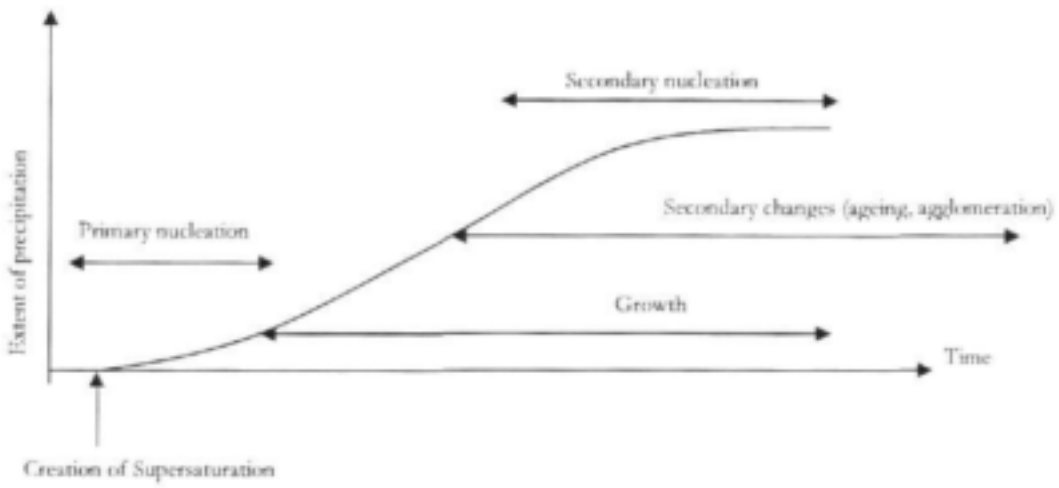

Figure 3: Individual steps involved in precipitation (Sohnel & Garside, 1992)

Physical aspects of precipitation

- **Effect of ionic concentration on precipitation product**

In any precipitation process, it is very unlikely that there will be a uniform stoichiometric distribution of the anions and cations. The level and ratio of the ion concentration determine the crystallisation mechanism and thus the nature of the precipitation products (Gosele & Kind, 1991). This is as illustrated in Figure 4.

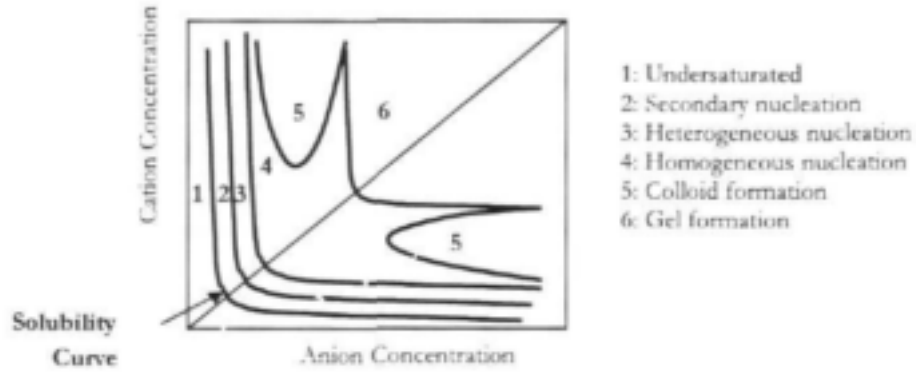

Figure 4: Effect of ionic concentration on nucleation (Gosele & Kind, 1991)

- **Particle Size Distribution**

Franke & Mersmann (1995) studied the continuous precipitation of gypsum using the reagents calcium nitrate and sodium sulphate. They found that the median crystal size is predominantly affected by primary nucleation, which increases strongly with supersaturation and is a very rapid mechanism.

Christoffersent *et al* (1982) and Liu & Nancollas (1970) prepared gypsum seed crystals using sodium sulphate and calcium chloride. Both studies showed that high concentrations result

in larger number of smaller (10-100 μm) particles whilst lower concentrations result in fewer, much larger, particles (30-200 μm).

O'Hern & Rush (1963) studied the precipitation of barium sulphate using barium hydroxide and sulphuric acid as reagents. Average particle size decreased from about 3μm with 0.01M and 0.02M reagents to 0.012 to 0.015 μm with 0.2M reagents. The effect of reagent concentration can be explained by the relative rates of growth and nucleation. For barium sulphate, nucleation rate increases with concentration to the eighteenth power. At lower concentrations nucleation is not so strongly dependent on concentration and growth may be the primary mechanism. The growth rate of barium sulphate increases with concentration to the fourth power at very low concentrations and to the first power at higher concentrations.

Non-stoichiometric precipitation can also affect particle size distribution. Wong *et al* (2001) studied the non-stoichiometric precipitation of barium sulphate. The feed consisted of sodium sulphate and barium chloride. $BaCl_2$ was kept as a limiting reagent of concentration 0.1M that was added to the sodium sulphate at a concentration ranging from 0.0018M to 0.027M, thus giving total molar ratios from 1/15 :1 or 1: 1/15 respectively. The results obtained were not symmetrical. The largest mean crystal size (~20-30 μm) was obtained when molar ratios close to 1 and $BaCl_2$ was used as the feed. This is in contrast to ~10-15 μm when Na_2SO_4 was used as the feed. For ratios 1/15 ($BaCl_2$ feed) and 15/1 (Na_2SO_4 feed), the mean sizes were much smaller and very similar (~3-5 μm).

* **Crystal morphology**

The shape of the crystal is largely determined by crystal growth. If surface reaction controlled growth takes place at lower supersaturation, crystals of compact shape such as cubes and octahedrals are formed (Sohnel & Garside, 1992). On the other hand, if the growth is largely anisotropic, elongated shapes such as needles, rods and plates are formed.
Franke & Mersmann (1995) identified the location of the reagent feed point as another parameter influencing formation of crystals with differing morphologies.
Lash & Burns (1984), in their experimental procedure, prepared calcium sulphate using stock solutions of H_2SO_4 and $CaCl_2$. They found that, at room temperatures (23°C), from solutions whose initial concentration (where the stated concentration of the solutions always refers to the calculated molarity based on $CaSO_4$ at the moment of mixing, before any precipitation occurred) is greater than 0.4M in $CaSO_4$, exothermic precipitation occurs. For solutions whose initial $CaSO_4$ concentration was less than 0.25M, the crystallisation was endothermic. Under microscopic examination the exothermically produced gypsum crystals appeared as very thin needles, while the endothermic crystals were platelets.

Christoffersen *et al* (1982) studied various morphologies and kinetics. In one experiment, crystals were prepared by drop-wise addition of stoichiometric amounts of Na_2SO_4 and $CaCl_2$, resulting in a 0.3M gypsum solution. These crystals were elongated with lengths varying from 30 to 200 μm. Many small crystals were also attached in parallel or twinned positions to the larger ones. In another experiment, crystals formed by the addition of equal volumes of $CaCl_2$ and Na_2SO_4 solutions resulting in a 0.725M gypsum solution had a much smoother surface with sizes varying from a length of 10 to 100 μm.

Liu & Nancollas (1970) studied the crystallisation of gypsum by the addition of seed crystals to stable supersaturated solutions at various temperatures between 15 and 45°C. The seed crystals that were prepared by the dropwise addition of $CaCl_2$ to Na_2SO_4 resulting in a 0.1M gypsum solution, were needle-like monoclinic crystals that were 80-120 µm in size. Other seed crystals prepared using 0.6M solutions were 30-50 µm in length.

Seeded Precipitation

Precipitation at low supersaturation levels is relatively slow and can be induced by seeding the solution. Kinetic relations for the growth of seed crystals from solution are fairly well established:

$$-\frac{dC_A}{dt} = kr\left(C_A - C^*\right)^n \qquad (2)$$

where:
k is a constant ($L^3/(mol^{-1}s)$)
r is the number of seed crystals
(C_A-C^*) is the excess solute concentration (mol/L),
n is the order of growth.

The number of seed crystals affects the growth rate either through the:

- Total surface area as in a surface- reaction phenomenon, or
- Surface-active sites as with screw dislocations

Bremere *et al* (1999) stated that desupersaturation is a decrease from influent concentration to a lower effluent concentration and that this can be achieved in a desupersaturation unit using seed crystals. Once the supersaturated solution is introduced into the unit, sparingly soluble salts automatically precipitate on active centres of the crystal lattice and create new active surface area. Supersaturation will dictate the rate of crystal growth and also the surface area and reactivity of the seeds. Obviously, changing the volume of seeds added will alter the total surface area of seed crystals and thus the global growth rate. Reactivity of crystals also depends on key growth sites on the surface, for example flat terraces and kink sites formed from incomplete regions on steps. Rough surfaces lead to faster growth rates. On the other hand, adsorption of impurities, antiscalants and organic matter, even at low concentrations, can inhibit crystal growth kinetics.

Verdoes & Hanemaaijer (1996) found that, at low supersaturation, seeded precipitation resulted in large crystals. Seeds can be either from the same material as the precipitate or from a foreign material. When seeds are from the same precipitate material, then precipitation occurs mainly by growth of the seed crystals, one disadvantage being that precipitation happens only on the active growth sites of the seeds and thus the active surface area available for precipitation is relatively small. When foreign seeds are used, precipitation is dominated by heterogeneous nucleation. The energy barrier for this process at low to intermediate supersaturation is lower than for homogeneous nucleation, which becomes dominant at higher supersaturation. Foreign seed precipitation has an advantage of the ability to control the active surface area available for precipitation by means of the particle size and the surface roughness of the seeds. In their research, Verdoes & Hanmaaijer (1996) studied the effect of seed size on crystallisation kinetics for the precipitation of calcium

carbonate. They found that precipitation on smaller seeds is measurably faster than on large sand seeds, thus proving the accelerating effect of the available surface area.

Liu & Nancollas (1973) studied the seeded crystal growth of gypsum from supersaturated solution and found a reaction second order in relative supersaturation. The effects of potential scale inhibitors including methyl enephosphoric acid and methylene phosphoric acid on the seeded growth of gypsum from supersaturated solutions were also studied (Liu and Nancollas, 1975). It was found that, in the presence of trace amounts of these additives, complete inhibition of growth for a certain period was achieved and thereafter the precipitation rate followed a second order law. They found that the duration of induction time (time for initiation of precipitation) was significantly affected by the amount of seed crystals added.

Seeded precipitation of gypsum from supersaturated solutions both in pure water and in the presence of sodium chloride was studied by Brandse *et al* (1977). They utilised 10% by volume of seed crystals and they plotted the mean linear growth rate, R against the relative supersaturation, σ. The relation between R and σ was given by a linear law for low values of σ. For higher values of σ a parabolic law was obtained and for very high values of σ growth rate was related by orders higher than two. They also found that the presence of sodium chloride in the precipitating system significantly increased the precipitation rate.

Seed preparation is an important step in seeded precipitation. Christoffersen *et al* (1982) experimented with seeded gypsum precipitation using six batches of gypsum seed crystals. These seed crystals were prepared in different ways and had different specific surface areas and sizes. Their results showed that the rate of growth varied for the different preparations of the gypsum seed crystals and that the overall rate of growth decreased with increasing mass of the crystals.

Role of mixing in precipitation

Mixing is used to reduce nonuniformalities or gradients in compositions, properties or temperature of material in bulk. Hydrodynamics and mixing have a critical role to play in chemical reactions as they affect the mixing of reagents that form the precipitate. Both nucleation and growth kinetics are often greatly influenced by the hydrodynamic conditions prevailing (Sohnel & Garside, 1992). Nagata (1975) stated that in nickel precipitation, seeds have to be suspended to maximise the surface area for precipitation as well as to make the bulk solution concentration more homogeneous.

O'Hern & Rush (1963) carried out a detailed study on the influence of stirring on precipitation. The findings showed that the precipitation rate, as well as the average size of the particles formed and the width of the size distribution, all depend on the manner and rate at which the reacting solutions are mixed together. The faster the solutions were mixed, the higher was the precipitation rate and the smaller the average particle size and narrower the crystal size distribution.

Torbacke & Rasmuson (2001) investigated the influence of mixing intensity on the crystal characteristics and found that increased mixing intensity leads to larger product crystals, contradicting the findings of O'Hern & Rush (1963). Their explanation to their results is that

increased agitation increases local mixing with the available bulk solution. Increased propeller agitation provides more bulk solution to the feed point region, which can be mixed with the feed.

Wong *et al* (2001) found that the impact of agitation speed on the precipitation had a generally small impact on the mean crystal size distribution of the barium sulphate size distribution. Only when barium chloride solution was fed at total molar ratios close to stoichiometric, the crystals became larger and their mean size was reduced by increased mixing intensity.

* **Reactor design**

To achieve good solid-liquid suspension in a reactor, and hence provide efficient precipitation process, a reactor has to be carefully designed. Physical aspects of the reactor can enhance solid-liquid suspension, including impeller type and tank geometry.

Impeller Type

Oldshue (1983) stated that for most effective solid suspension, axial-flow impellers are best to use amongst the impeller types. Less impeller speed is required to drag the particles off-bottom of the reactor for suspension when axial impellers are used. Axial impellers induce axial flow, which induce high fluid flow rate with lower shear rate. The fluid flows in either a top-to-bottom pattern for down-pumping impellers or bottom-to-top pattern for up-pumping impellers. He also stated that multiple impellers should be used when liquid height is larger than the tank diameter, to maintain a full top-to-bottom flow pattern, thus utilising the full depth of liquid. Harnby *et al* (1992) stated that axial flow impellers require the least power input compared to the other impeller types. For a maximum flow to shear ratio, Oldshue (1983) stated that the impeller diameter should be one third of the tank diameter. The clearance from the bottom to the impeller should also be a third of the liquid height.

Tank geometry

Turbulence is important to achieve good mixing. Various geometric improvements of the internals of the vessel help to break up circulatory flow to produce turbulence and reduce the formation of vortex. The following are the parameters studied:

- Baffles. These interrupt the flow circulation and create turbulence in the fluid. Conventional design states baffle widths at 1/10-1/12 of the tank diameter are usually enough to generate top-to-bottom mixing to reduce vortexing and swirling (Doran, 1995). Nagata (1975) stated that the vertical circulatory flow in a baffled tank is four times as large as that in an unbaffled tank.
- Draft tubes. These improve axial flow movement from the impeller. Because of the increased volume of re-circulating down-pumping fluid, the impeller is subject to increase of velocity heads (Uhl and Gray, 1966). Oldshue (1983) states that draft tubes ensure top-to-bottom flow for all tanks with height of liquid larger than tank diameter, and also decrease the tendency of solid deposition by sweeping the solids away from the draft tube. Harnby et al (1992) found that care should be taken with the position and size of the draft tube. Ideally, the flow area in the core, in the annulus, between the bottom of the tube and the base and between the top and the liquid surface should all be equal.
- Bottom geometry. For flat-bottomed vessels, with down pumping impellers, it has been seen that solids form dead zones in the corners of the vessel. To eliminate fillet

formation, rounded edges are employed or the vessel fitted with a dished bottom (Nagata, 1975). The off-bottom clearance can be set between a quarter and a third of the liquid height is standard where the total liquid level is as given in equation (3)

$$H = n'T \tag{3}$$

Where:

n' is the number of impellers
T is the tank diameter (m).

* **Reactor hydrodynamics and dimensional analysis**

The general dimensionless equation considers the impeller power as a function of the geometry of the impeller and the tank, the properties of the fluid (viscosity and density), the rotational speed of the impeller, and gravitational force. The Buckhingham Pi theorem gives the following general dimensionless equation for the relationship of the variables:

$$f\left(\frac{D^2N\rho}{\mu}, \frac{DN^2}{g}, \frac{Pg}{\rho N^3 D^5}, \frac{D}{T}, \frac{D}{Z}, \frac{D}{c}, \frac{D}{p}, \frac{D}{w}, \frac{D}{l}, \frac{n_2}{n_1}\right) = 0 \tag{4}$$

where D = impeller diameter (m),
T = tank diameter (m),
Z = liquid depth (m),
c = clearance of impeller off vessel bottom (m),
W = impeller width (m),
p = pitch of blade,
n_1 = number of blades,
l = blade length (m),
ρ = density (kg/m^3),
μ = viscosity (kg/ms),
P = power (W),
N = impeller rotational speed (rps),
g = gravitational acceleration (m/s^2).

The last seven terms in equation (4) represent the condition of the geometric similarity, which requires that all corresponding dimensions in systems of different size bear the same ratio to each other. Confining the discussion to geometrically similar systems, equation (4) may be stated as

$$f\left(\frac{D^2N\rho}{\mu}, \frac{DN^2}{g}, \frac{Pg}{\rho N^3 D^5}\right) = 0 \tag{5}$$

The first group in equation(5), $\frac{D^2N\rho}{\mu}$, is the Reynolds number, N_{RI}, and represents the ratio of inertial forces to viscous forces. This ratio determines whether conditions of the flow are turbulent or laminar and is thus a critical group in the correlating power. If the

Reynolds number is less than or greater than 10^4 the flow is considered to be laminar and turbulent respectively.

The second group in equation(5), $\frac{DN^2}{g}$, is the Froude number, N_{Fr}, and represents the ratio of inertial to gravitational forces. This term can be unimportant in flow problems, but in the case of unbaffled tanks where vortexing occurs, the shape of the vortex represents a balancing of gravitational and inertial forces.

The third group in equation(5), $\frac{Pg}{\rho N^3 D^5}$, is the Power number, N_P, and represents the ratio of pressure differences producing flow to inertial forces. (Uhl & Gray, 1966)

* **Mixing time scale analysis**

The complex process of turbulent mixing can be broken down into simpler mixing steps, macro mixing, meso mixing and micro mixing. Macro mixing the process of mixing that takes place on the scale of the whole vessel. Macro mixing defines residence time distributions and determines the environment concentrations for meso mixing and macro mixing. It also conveys fluids that are undergoing meso mixing and micro mixing through environments where turbulence properties (such as the rate of energy dissipation, ε, and the scale of turbulence, Λ_s) vary. Meso mixing represents the coarse-scale turbulent exchange between the fresh feed and its surroundings. This can be explained by the concept of a fast reaction whereby the reaction is localised near the feed point, forming a plume of fresh feed. This plume is coarse-scale relative to the micro mixing scales and is of fine-scale as compared to the scale of the system. Micro mixing happens on the molecular scale and can thus directly affect chemical reaction, nucleation and crystal growth, which are essentially molecular-level processes (Baldyga & Bourne, 1999). It has been experimentally found that, for a well-baffled tank and fully developed turbulence, the macro mixing time, τ_M, is between 3 and five times the circulation time, τ_c

$$\tau_M = 4\tau_c \tag{6}$$

For a vessel using an impeller with four pitched blades the mixing rate determining circulation time, τ_c, which is the macro mixing time, can be expressed as follows (Roelands *et al*, 2003):

$$\tau_c = \frac{V}{q_c} \tag{7}$$

Where:
V = vessel contents (m^3),
q_c = pumping capacity of the impeller (m^3/s).

The pumping capacity of the impeller is given by (Roelands *et al*, 2003):

$$q_C = 1.5ND^3 \tag{8}$$

Where:
N = impeller speed (rps),
D = impeller diameter (m).

The meso mixing time is determined as (Torbacke & Rasmuson, 2001):

$$\tau_{meso} = a\left(\frac{\Lambda^2}{\varepsilon}\right)^{1/3} \tag{9}$$

Where:
a = constant (given as 2 (Baldyga et al, 1997)),
Λ = macroscale turbulence (m),
ε = local energy dissipation rate (m^2/s^3).

The macroscale turbulence is estimated (Torbacke and Rasmuson, 2001) as:

$$\Lambda = \sqrt{\frac{Q_b}{\pi u}} \tag{10}$$

Where:
Q_b= Reactant flow rate (m^3/s)
u = fluid velocity (m/s)

The local energy dissipation rate is given by (Torbacke and Rasmuson, 2001):

$$\varepsilon = a\frac{N_p N^3 D^5}{V} \tag{11}$$

Where:
a = constant (given as 2 (Baldyga et al, 1997)),
N_p = power number (taken as 1.5 for a pitched blade (Uhl and Gray, 1966)),
N = impeller speed (rps),
D = impeller diameter (m),
V = reactor contents (m^3).

The micro mixing time is determined as (Baldyga and Bourne, 1989):

$$\tau_{micro} = 17.24\sqrt{\frac{\gamma}{\varepsilon}} \tag{12}$$

Where:
γ = kinematic viscosity (m^2/s),
ε = local energy dissipation rate (m^2/s^3)

4.4. Membrane Technology Review

(Coulson & Richardson, 1997)

In a membrane separation process, as depicted in Figure 5, the feed stream consisting of two or more components is pumped tangentially across the membrane. The membrane separates

this stream into a purified effluent stream (permeate) and a stream (retentate) more concentrated in solute, the ions of which are too large to pass through the membrane pores.

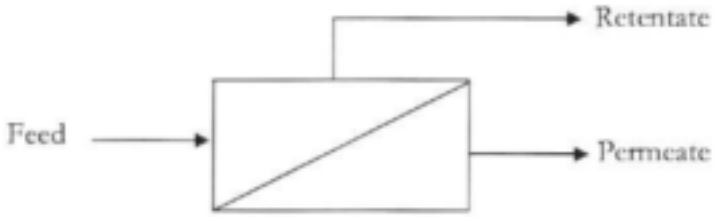

Figure 5: General Membrane Process

Industrial membrane processes may be classified according to the driving force used in the process and the size range of materials to be separated. Both ultrafiltration (UF) and Reverse Osmosis (RO) membranes use pressure gradient as the driving force. The typical operating pressure and size range of materials separated for various membrane processes are shown in Table 4:

Table 4: Typical operating pressure and size range of materials separated for UF and RO systems

Membrane process		Pressure range [Bar]	Size range of particles removed [µm]
Reverse Osmosis	(RO)	3.4-69	0.0001 – 0.001
Nanofiltration	(NF)	2.0-40	0.0005 – 0.005
Ultra filtration	(UF)	0.7-6.9	0.005 – 0.05
Microfiltration	(MF)	0.3-1.7	0.1 – 10

Membranes used for the pressure driven processes, microfiltration, ultrafiltration and reverse osmosis are most commonly made of polymeric materials such as polyamide, polysulfone and polycarbonate. Ultrafiltration and reverse osmosis membranes are characterised by an asymmetric structure with a 1-2 µm thick top layer of finest pore size supported by a 100 µm thick, more openly porous matrix.

4.5. Reverse Osmosis

Reverse osmosis (as illustrated in Figure 6) processes operate at elevated pressures. Thermodynamically, for solutions on either side of a membrane to be in osmotic equilibrium, their chemical potentials must be equal. Pure water has a higher chemical potential than a solution, indicating that a system consisting of pure water on one side of a membrane and a solution on the other will result in the transport of the pure water through the membrane into the solution i.e. in the direction of lower chemical potential. Increasing the pressure on the solution side would increase its chemical potential and restore the osmotic potential whilst at higher pressures; it would force the water to flow through the membrane. This process is called reverse osmosis. (Seader and Henley, 1998)

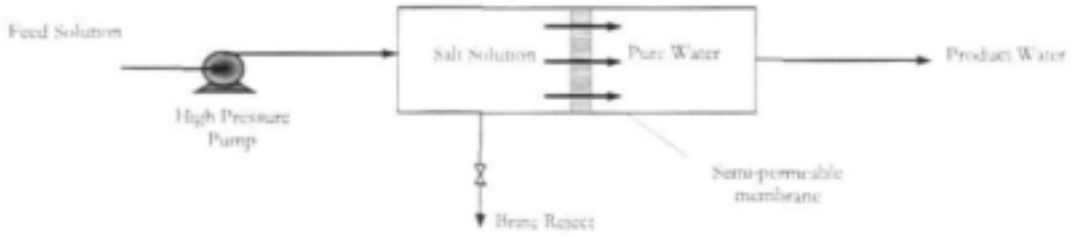

Figure 6: Principles of Reverse Osmosis

The minimum exit pressure from the module is 2000kPa. The reactor can be operated at 2000kPa and, by doing so the cost of energy required to pump the feed solution from atmospheric pressure to the reactor operating pressure can be saved. At the same time, the savings in the pumping costs would not offset the capital costs associated with the pressurised reactor system. In his research, Juby (1994) chose to use atmospheric pressure for the operation of the reactor. For smooth operation of the SPARRO process, the settling of gypsum crystals has to be avoided. For simplicity, Juby (1994) used a single mixed reactor for his pilot plant.

4.6. Concentration Polarisation

(Coulson & Richardson, 1997)

The separation of process liquid and solute that takes place at the membrane gives rise to an increase in solute concentration close to the membrane surface. This is termed concentration polarisation and takes place within the boundary film generated by the applied cross-flow as illustrated in Figure 7. The main effects of concentration polarization are a reduced solvent permeation rate as a result of an increased osmotic pressure at the membrane surface and a decrease in solute rejection. Both UF and RO membranes are susceptible to concentration polarisation effects, UF to a lesser extent than RO membranes.

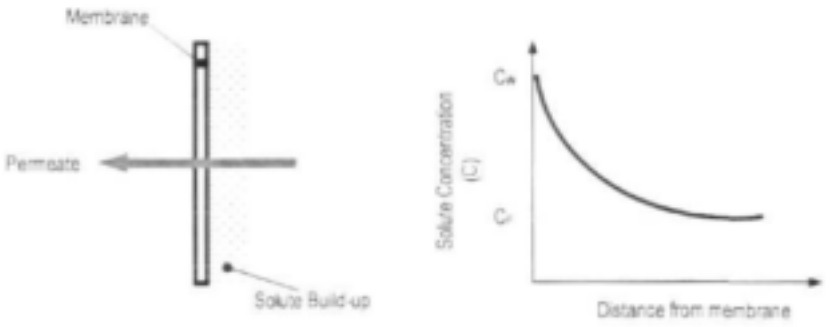

Figure 7: Concentration polarisation at a membrane surface (Coulson & Richardson, 1997)

Terminology

Rejection - a measure of the dissolved material that does not pass through the membrane.

Passage – a measure of the dissolved material that passes through the membrane.

Recovery - the ratio of permeate rate to feed rate.

$$\text{Recovery} = \frac{\textit{Permeate Rate}}{\textit{Feed Rate}} = \frac{Q_p}{Q_f} \tag{13}$$

5. SCOPING STUDIES

Preliminary research work focussing on producing gypsum crystals of predictable size and morphology investigated the effect of changing selected processing conditions on particle size distribution and crystal morphology.

It was possible to consistently produce both "platelets" and "needles" in an experimental situation where all parameters except the initial reagent concentration were kept constant. The effect of changing selected processing conditions (reagent concentration, reagent feed rate and stirrer speed) on particle size distribution and morphology was also examined. For the particle size distribution, a 2^3 factorial half replicate series of nine experiments was carried out and a first order model fitted to the results. It was found that reagent concentration had the greatest effect on the particle size distribution of the crystals obtained. A further nine experiments were carried out to examine the effect of the same processing parameters on morphology. Visual observations showed that reagent concentration also had the most significant effect on crystal morphology, with high reagent concentrations (equivalent to 14700mg/L gypsum) forming platelets and low concentrations (equivalent to 5880mg/L gypsum) forming needles.

The concentration of calcium (400mg/L) and sulphate (1850mg/L) in the raw mine water previously tested on the SPARRO process (Juby *et al.* 1994) suggests that gypsum crystals of needle type morphology will predominate. For the purposes of this investigation, it is necessary to be able to control both the crystal morphology and thus size, in order to be able to isolate the effects of these parameters on the process.

After the scoping studies, the investigation was divided into two parallel and interactive research thrusts:

- Design, building and commissioning of the SPARRO Membrane Test Rig (SMTR) mini plant and the Direct Slurry Spraying Technique (DSST) - this aspect of the research focussed on aspects of operation and control for the SPARRO process.
- Control of the desupersaturation reactor - this phase of the research focussed on the crystallisation aspects of the process.

6. Design, building and commissioning of a reverse osmosis membrane test system

The SPARRO Membrane Test Rig (SMTR) miniplant, shown in Figure 8 and Figure 9 below, is a single cellulose acetate membrane module through which a feed slurry with specific crystal characteristics is recycled in a closed loop circuit under specified operating conditions. The length of the tubular membrane used in the test rig was 0.55 m (as opposed to the complete length of 2.5m) in order to intensify the loading and potentially accelerate any membrane damage.

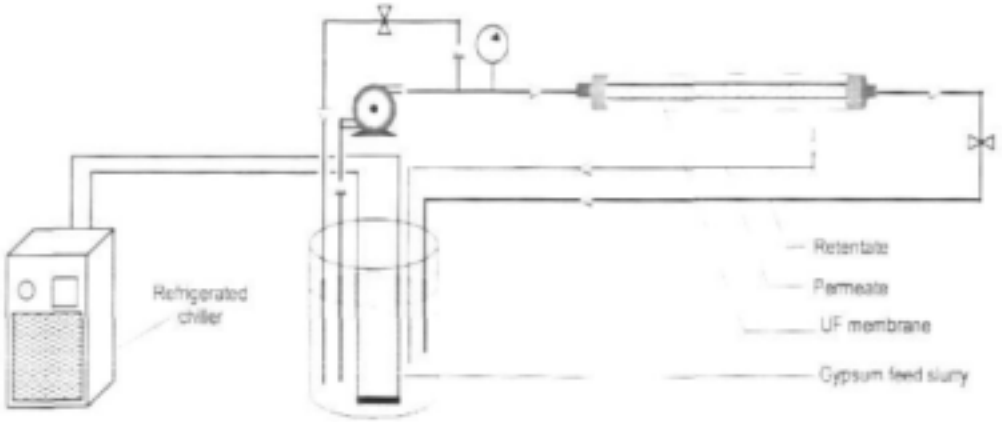

Figure 8: SPARRO Membrane Test Rig (SMTR) schematic

Figure 9: SPARRO Membrane Test Rig (SMTR) photograph

The aims of the SMTR were to investigate the effect that the different gypsum crystal characteristics, under conditions of turbulent flow within the membrane, have on membrane damage from a crystallisation perspective and the impact of slurry velocity on membrane damage from an operational perspective.

The system's performance was continually monitored by measuring the pressure and temperature normalised salt rejection based on the difference between the feed and permeate conductivities and permeate flux over time. Once a significant decrease in the membrane performance was detected, based on the permeate flux or conductivity based salt rejection, the membrane was removed and the surface analysed for damage using membrane staining techniques and differential interference contrast (DIC) reflected light microscopy or scanning electron microscopy (SEM).

A set of statistically designed experiments based on a response surface methodology (RSM), to ascertain the response of the system (system performance) as a result of changing particular system operating parameters was initiated. The experimental program involved varying the feed crystal morphology, slurry velocity and pH at the three levels shown in Table 5 below:

Table 5: Levels of factors varied in the statistical design

Factor	Level 1	Level 2	Level 3
Crystal shape	Needles	Needle – plates	Plates
Linear velocity [m/s]	0.70	1.25	1.80

After operating the SMTR for over 700 hours under operating conditions most likely to inflict membrane damage i.e. a feed slurry containing only crystals of needle morphology at the highest linear velocity of 1.80m/s, no significant decline in the membrane performance, that would be considered to be a deviation from normal performance levels, was detected. As a result, in line with suggestions proposed at the inaugural steering committee meeting, the following strategies were adopted in an attempt to accelerate the process.

6.1. Increased linear velocity and gypsum crystal concentration through membrane

In order to accelerate the effect of membrane damage and to obtain meaningful data within the time frame of this project, the linear velocity within the membrane was increased to a maximum of 2.44 m/s. This value was constrained by the pumping capabilities of the SMTR mini-plant. In addition, feed slurries containing higher seed crystal concentrations compared to those used in the 700 hour run were investigated in both continuous (24 hours/day) and intermittent (8 hours/day) operating mode.

Intermittent operation

Operating the SMTR in intermittent mode provided valuable information on the system performance subsequent to regular shut downs by allowing the membrane to remain in contact with seeded slurry during the shut down. Both sets of intermittent experiments (the first which involved a feed slurry containing gypsum crystals with a needle type morphology

and the second with a platelet type morphology) were operated at 4000 kPa, a linear velocity through the membrane of 2.44 m/s, a feed temperature of 22°C and a seed concentration of 2.14g/L. The effect of two different gypsum morphologies on the salt rejection and membrane flux for intermittent operation are shown below in Figure 10 for needle type morphology and Figure 11 platelet morphology.

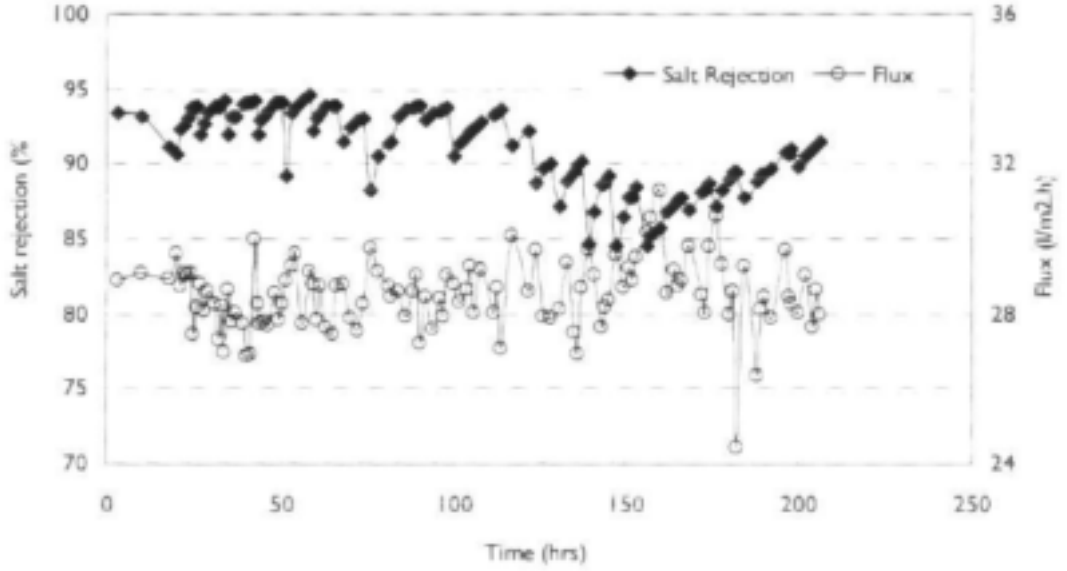

Figure 10: Effect of needle type morphology on salt rejection and membrane flux

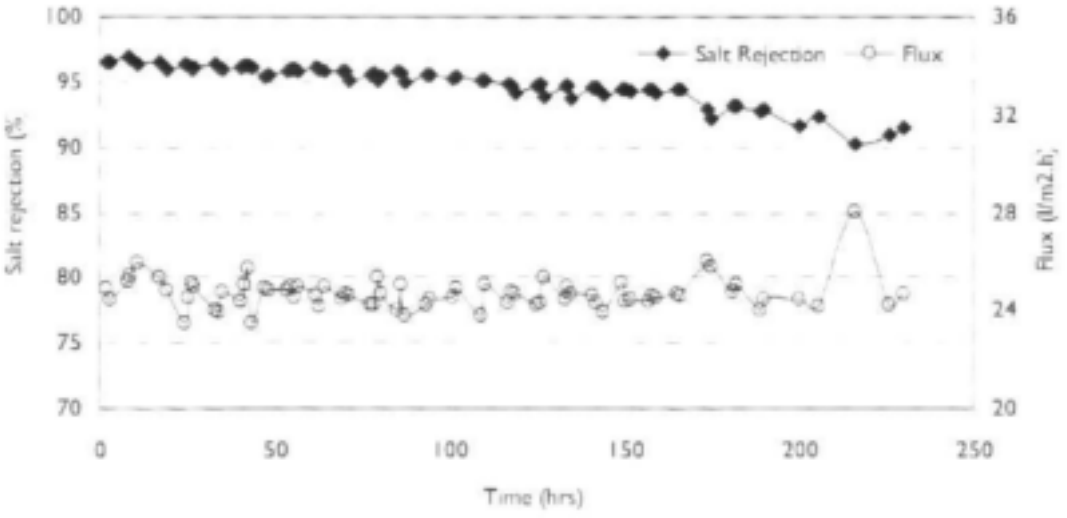

Figure 11: Effect of platelet type morphology on salt rejection and membrane flux

From the results above, it is clear that the needle type morphology has a greater detrimental effect on both salt rejection and membrane flux, with the system taking up to 8 hours to return to the normal performance levels subsequent to a shut down. Furthermore, the corresponding decrease in salt rejection as a result of a higher permeate flux is consistent with membrane theory. On the other hand, the platelet type morphology exhibited a lower detrimental effect on the performance of the system, with the system reaching normal performance levels within the first 2 hours of restarting the system in addition to maintaining relatively consistent salt rejection and permeate flux.

The negative effect of the needle type morphology is further evident in Figure 12 below, which shows the average salt rejection values obtained for the two types of morphologies for each 8 hour period for the duration of the experiment.

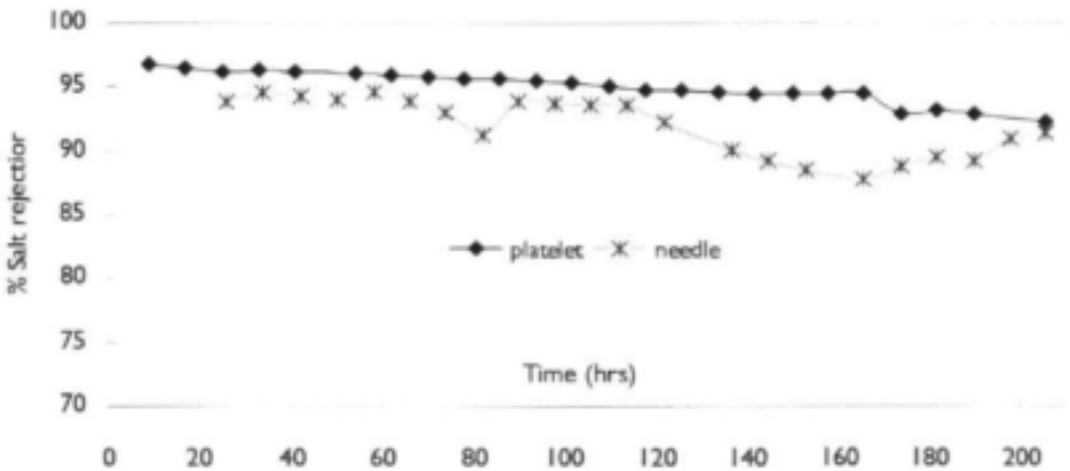

Figure 12: Effect of platelet and needle type morphology on average salt rejection

In conclusion, with regards to membrane damage and system performance when operating in intermittent mode, this mode of operation has provided some data on the effect of plant shutdowns on recovery time as well as conductivity based salt rejection and permeates flux. Although the process may not be shut down during normal operation with the same frequency as in this experiment, it is clear that the recovery time for the process to reach optimal operating specification in terms of salt rejection and permeate flux are significantly greater in the presence of needle type morphology as compared to platelet type. However, no significant conclusions can be drawn from these findings with regards to any of the two morphologies having a significant influence on membrane damage.

Continuous operation

Three sets of continuous experiments were performed: two with feed slurries containing gypsum crystals of needle type morphology and the third with platelet morphology. All experiments were operated at 4000kPa, a linear velocity through the membrane of 2.44m/s, a feed temperature of 22°C and a seed concentration of 2.14g/L. The effect of gypsum morphology on salt rejection and membrane flux for continuous operation are shown below for needle type morphology (Figure 13 and Figure 14) and platelet morphology (Figure 15).

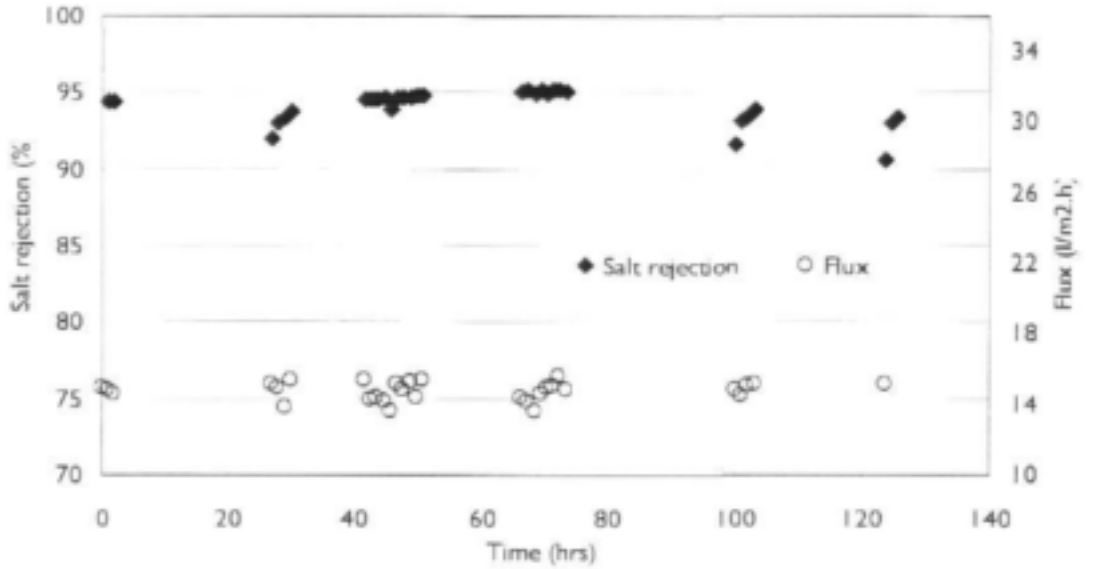

Figure 13: Effect of needle type morphology on salt rejection and membrane flux

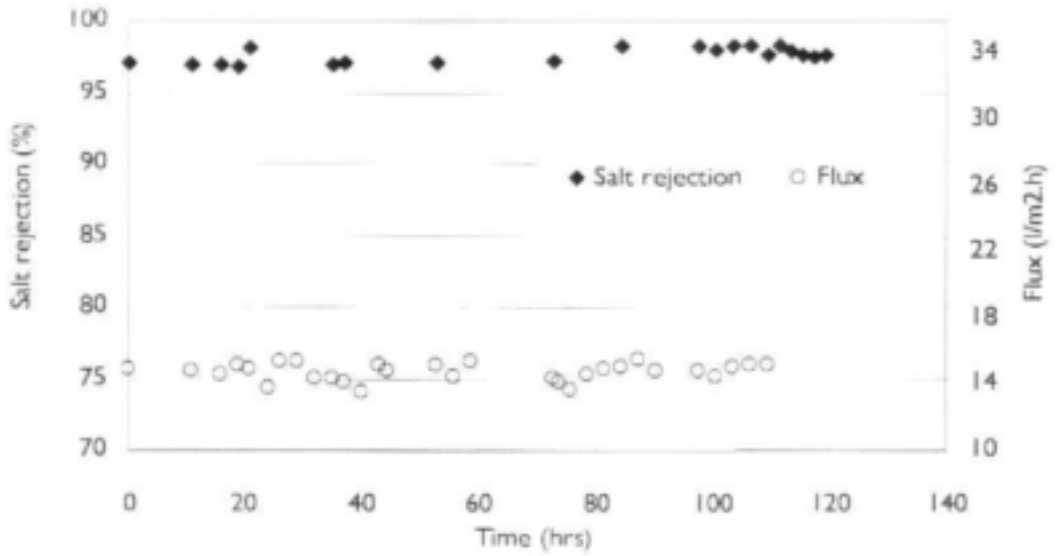

Figure 14: Effect of needle type morphology on salt rejection and membrane flux

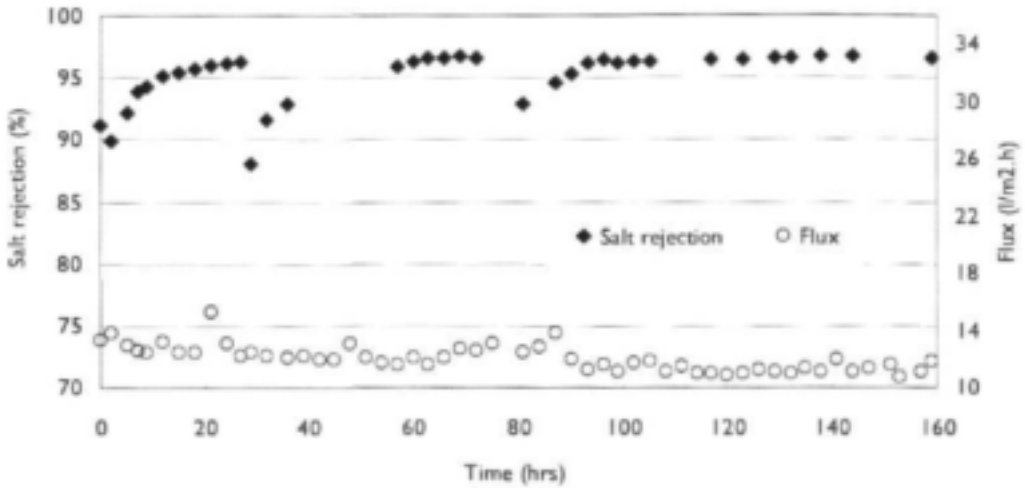

Figure 15: Effect of platelet type morphology on salt rejection and membrane flux

Comparing the results shown in the graphs above, it is evident that the needle morphology shows a greater degree of variability in salt rejection and membrane flux than the platelets, which gave a salt rejection consistently at or around 96%, except for a brief period after the twenty first and eightieth hour of operation, when the SMTR mini-plant had to be temporarily shut down for maintenance.

Though the continuous mode of operation does give some indication that the needle type morphology is more detrimental to membrane performance in terms of operational variability, the evidence is not conclusive.

Continuous operation with high seed concentrations

This final phase of the work was aimed at investigating the effect of an even higher seed concentration (14g/l), similar to the concentrations found further down the SPARRO modules during normal operation with the continuous removal of water along the length of the module.

Initially, a standard salt test was performed so as to obtain a typical performance reference curve for the cellulose acetate membranes, which provided a base line against which any variations as a result of the different morphologies could be measured for this phase of the work as well as the previous experimental work described above. The standard salt test experiment was carried out with NaCl, at an operating pressure of 4000kPa, a linear velocity through the membrane of 2.44m/s, a feed temperature of 22°C and a feed conductivity of 14mS/cm. The results of this test are shown in Figure 16 below:

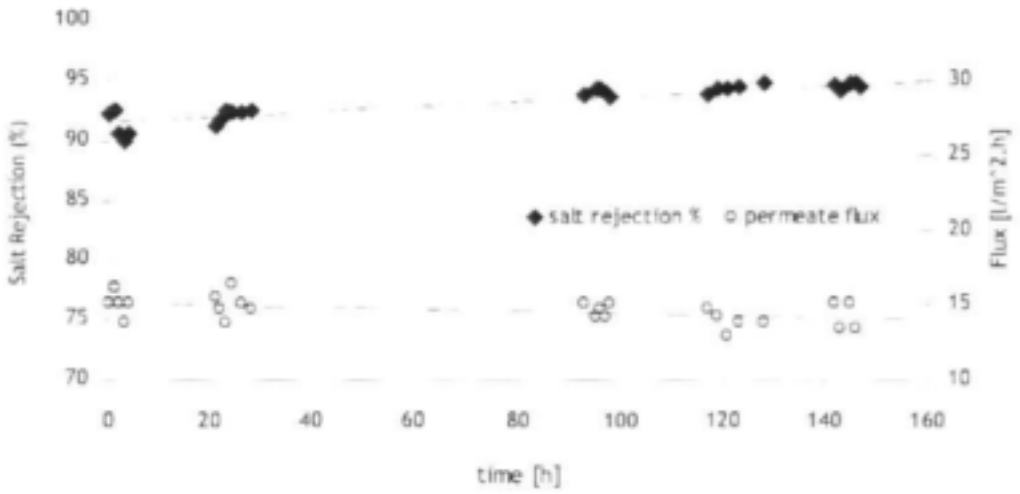

Figure 16: Standard salt test – effect of NaCl solution on salt rejection and membrane flux for a cellulose acetate RO membrane

Results above show that after 160 hours of continuous operation, there is no significant decline in the conductivity based salt rejection. In fact, the salt rejection tends to increase slightly, with an expected corresponding decrease in the flux indicating the formation of cake layer and therefore an increased resistance to the diffusion of solute through the membrane pores.

Importantly, the relatively flat profile of the reference curve for the cellulose acetate RO membrane eliminates an inherent membrane performance decline with time as a possible reason for the deviations reported previously and consequently, places the focus on either the characteristics of the feed morphology or operating conditions, at least for a 160 hour time frame.

Two sets of continuous experiments with a high seeds concentration of 14g/l were performed: one with feed slurries containing gypsum crystals of needle type morphology and the other with platelet type morphology. All experiments were carried out at a pressure of 4000kPa, a linear velocity through the membrane of 2.44m/s and a feed temperature of 22°C. The effect of gypsum morphology on salt rejection and membrane flux are shown below for needle type morphology (Figure 17) and platelet morphology (Figure 18).

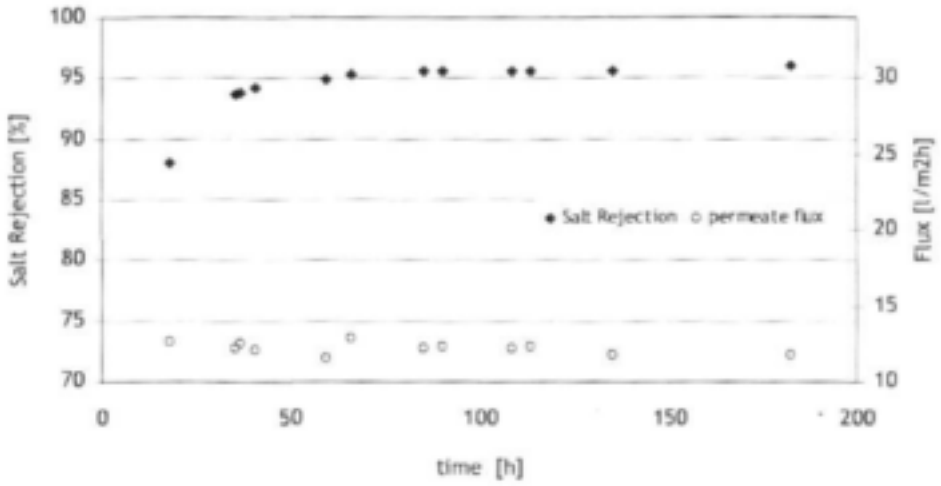

Figure 17: Effect of needle type morphology, high seeds concentration on salt rejection and flux.

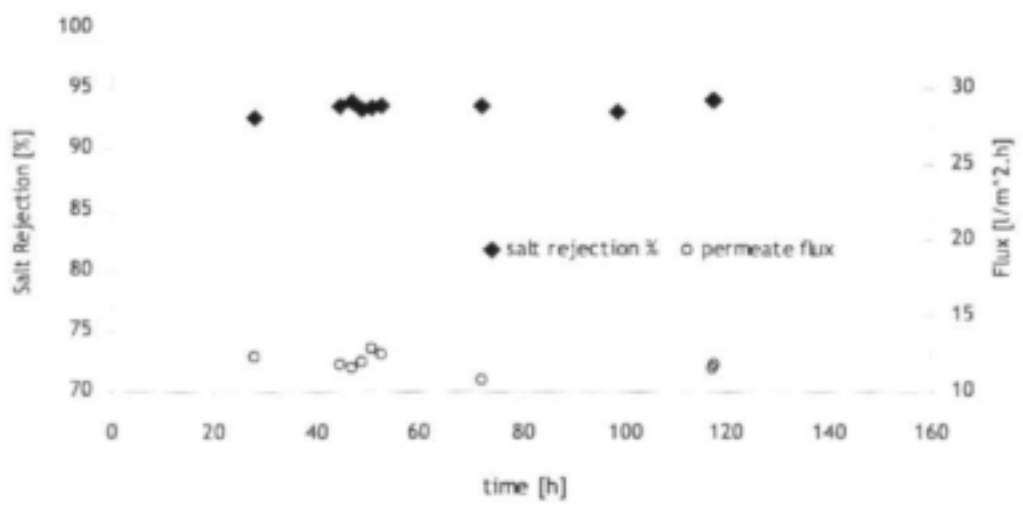

Figure 18: Effect of platelet type morphology, high seeds concentration on salt rejection and flux.

Comparing the salt rejection profiles in Figures 17 and 18 with the standard salt solution profile in Figure 16, it can be seen that there is no noticeable significant variation in the salt

rejection over time that would be indicative of membrane damage having occurred for either a needle or platelet type morphology. Whereas, the duration of these experiments was shorter than the typical total operating time for a membrane module at full scale operation; it is expected that the more abrasive conditions (as a result of a higher seeds concentration and linear velocity through the membrane) under which the SMTR mini-plant was operated, would have shown signs of a deterioration in membrane performance if morphology has an influence on membrane damage.

Consequently, the directed slurry spraying technique (DSST) described in section 1.2 below was developed to confirm whether or not gypsum crystal morphology has the potential to cause membrane damage through abrasion.

6.2. Directed slurry spraying technique (DSST)

This method of accelerating the investigation of membrane damage due to crystal scouring is based on directing a slurry stream of gypsum crystals at varying angles onto an exposed membrane surface. The directed slurry spray method exposes the membrane to the most extreme scouring conditions, even compared to industrial operating conditions. This was intended to clarify whether or not gypsum crystal morphology could have any impact on membrane damage.

The directed slurry spraying technique (DSST) apparatus consists of three membrane surfaces, each simultaneously sprayed by a feed slurry (with specific crystal characteristics) being recycled in a closed loop circuit under specified operating conditions. The operating variables include the angle of impact, the velocity through the spray nozzles and the crystal morphology of the feed. A schematic diagram of experimental apparatus is shown below:

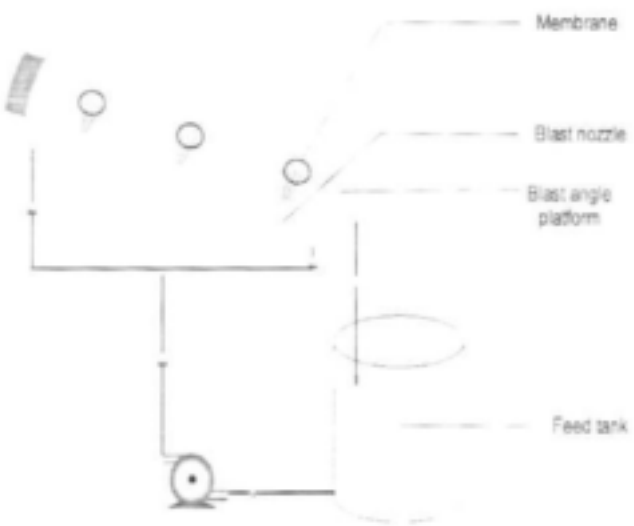

Figure 19: Schematic diagram of directed slurry spraying apparatus

The feed slurry is dosed with a small quantity of Congo Red indicator, which serves to stain the membrane surface at any point where damage occurs, providing a simple method for determining when the membrane should be removed for damage analysis.

Feed slurries of either a needle or platelet type morphology were synthesised in accordance with conditions specified by Lewis *et al* (2002). In each case, 18 litres of feed slurry were prepared in batch mode by continuously adding equimolar quantities of $CaCl_2$ and Na_2SO_4 to a stirred tank maintained at a temperature of 25°C. A 0.04M solution of $CaSO_4$ produced a feed slurry containing crystals of needle type morphology, while a 0.5M solution of $CaSO_4$ produced the platelet type morphology. In each case, the residence time in the reactor was 16 hours.

The concentration of crystals in the slurry feed was 6.2g/L. In the case of the feed containing needle morphology, due to the significantly lower $CaSO_4$ concentration, the required mass of crystals was accumulated by preparing a number of batches and combining them in a 0.04M mother liquor solution.

After exposure to the slurry spraying for the required time, the membranes were removed and immediately soaked in deionised water to minimise any possibility of membrane hydrolysis through dehydration. Before observing the membranes under a scanning electron microscope (Leica S440), $1cm^2$ of the exposed membrane surface, encompassing the epicentre of the region of contact between the slurry stream and the membrane was cut, placed on the stub and immediately submerged into liquid nitrogen to preserve the membrane surface characteristics and avoid membrane hydrolysis.

The experiments were carried out at spraying angles of 90° and 45°. Twelve sets of experiments were carried out as outlined in Table 6 below:

Table 6: Experimental operating conditions

Experiment no	Crystal morphology	Linear velocity through nozzle	Spraying angle	Nozzle to membrane distance	Mass of Congo Red indicator	Duration of experiment
1	Control – water only	$4.5ms^{-1}$	90°	4cm	0.22g	70 hours
2	Control – water only	$4.5ms^{-1}$	90°	4cm	0.22g	70 hours
3	platelets	$4.5ms^{-1}$	90°	4cm	0.22g	70 hours
4	platelets	$4.5ms^{-1}$	90°	4cm	0.22g	70 hours
5	needles	$4.5ms^{-1}$	90°	4cm	0.22g	70 hours
6	needles	$4.5ms^{-1}$	90°	4cm	0.22g	70 hours
7	Control – water only	$4.5ms^{-1}$	45°	4cm	0.22g	70 hours
8	Control – water only	$4.5ms^{-1}$	45°	4cm	0.22g	70 hours

9	platelets	$4.5ms^{-1}$	45°	4cm	0.22g	70 hours
10	platelets	$4.5ms^{-1}$	45°	4cm	0.22g	70 hours
11	needles	$4.5ms^{-1}$	45°	4cm	0.22g	70 hours
12	needles	$4.5ms^{-1}$	45°	4cm	0.22g	70 hours

a) Effect of deionised water and Congo Red on membrane damage: control experiment

This set of experiments was carried out as a control. Figure 20 shows an SEM of a new, unused membrane surface and Figure 21 shows the results of the control experiment.

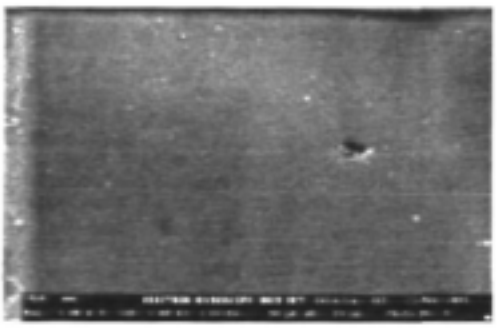

Figure 20: New, unused membrane surface (Scale bar=10μm)

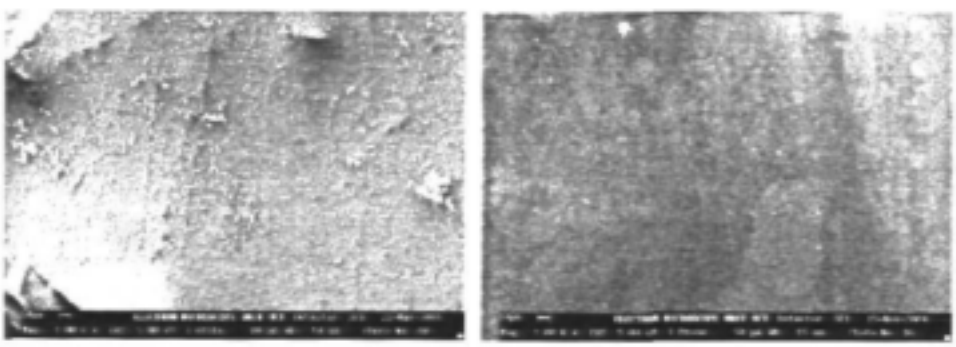

Figure 21: Control experiment: Membrane surface sprayed at 90° (left) and 45° (right) with only deionised water and Congo Red

(Scale bar=10μm)

The results show that there is insignificant scouring damage of the membrane surface caused by water or Congo Red alone.

b) Effect of platelet type morphology on membrane damage

Figure 22 and Figure 23 show SEMs of the most damaged region within the $1cm^2$ epicentre of contact between the slurry spray and the membrane surface from experiments 3, 4, 9 and 10 indicating the impact of the platelet type morphology on membrane damage at spraying angles of 90° and 45° respectively.

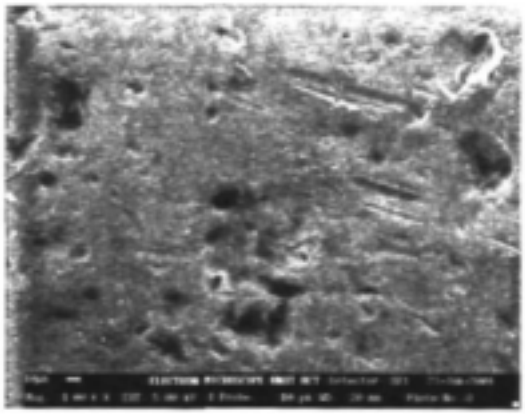

Figure 22: Most damaged membrane surface as result of being sprayed at 90^0 with feed slurry containing platelet type gypsum morphology

(Scale bar=10μm)

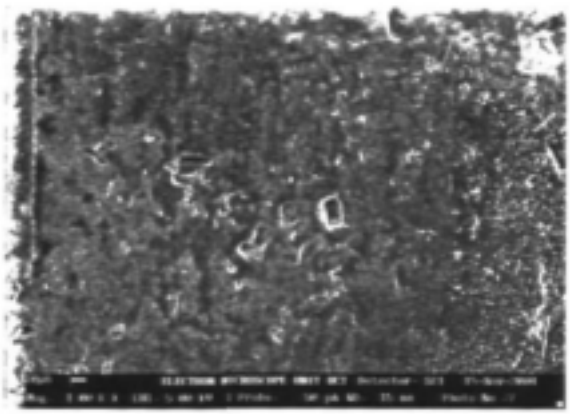

Figure 23: Most damaged membrane surface as result of being sprayed at 45^0 with a feed slurry containing platelet type gypsum morphology

(Scale bar=10μm)

The results of spraying the membrane surface with a feed slurry containing the platelet type morphology crystals at a spraying angle of 90°, shows that after 70 hours of exposure to the spray, the membranes do not show signs of major damage. In addition, it is clear that there is significantly less damage at a spraying angle of 45°.

c) Effect of needle type morphology on membrane damage

Figure 24 and Figure 25 show SEMs of the most damaged region within the 1cm^2 epicentre of contact between the slurry spray and the membrane surface from experiments 5, 6, 11 and 12 indicating the impact of the needle morphology crystals on membrane damage.

Figure 24: Most damaged membrane surface of the most damaged region within the 1cm^2 epicentre of contact between the slurry spray and the membrane surface as result of being sprayed at 90° with a feed slurry containing needle type gypsum morphology

(Scale bar=10μm)

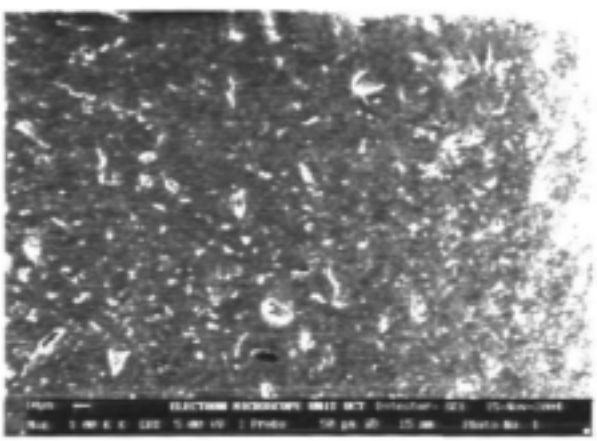

Figure 25: Most damaged membrane surfaces as result of being sprayed at 45° with a feed slurry containing needle type gypsum morphology

(Scale bar=10μm)

Based on the results shown above, it is clear that for both morphologies the extent of damage due to scouring is significantly less at a spraying angle of 45°. This angle would be more representative of the angle of impact of the crystals with the surface in normal operation. Figure 24 and Figure 25 show that, the damage caused by the needle type morphology is significant compared to the platelet type morphology.

The results presented above show that this novel accelerated approach to investigating the effect of gypsum crystal morphology on membrane damage in the SPARRO process provides useful qualitative information. The major conclusion is that crystal morphology has the potential to play a significant role in membrane damage, with the needle type morphology having a significant impact on membrane damage compared to the platelet type morphology.

The implications of this work are that, if the platelet morphology of the crystals in the SPARRO process is maintained, membrane damage is expected to be reduced.

6.3. Testing of membranes from Sasol Secunda's RO plant

In an attempt to investigate the effect of gypsum scaling on a full scale reverse osmosis plant, a batch of used membranes from Sasol's Secunda RO plant were obtained with the assistance of Weir Techna. A module from the back end of the process was tested. This is where the greatest extent of damage to the membrane surface would be expected due to the concentration of the suspended solids being the highest at this point. Scanning electron microscopy failed to reveal any signs of membrane surface deterioration due to scouring on all the membranes tested.

6.4. Pump performance related issues

According to Juby (1994), the high pressure multistage centrifugal pumps used in Phase I of the previous work failed after 600 hours as a result of extreme wearing down of the plastic impellers. These pumps were unsuitable for pumping slurries and consequently replaced in Phase II by triplex plunger pumps which performed satisfactorily except for poor sealing between the plunger and the packing with time.

After consultation with Weir Techna (Membratek) (Paarl), it was established that the triplex plunger pumps e.g. Hydracell Model D10, which was used for this research, function optimally with seed concentrations up to 6g/Litre and exhibit poor sealing characteristics at higher concentrations such the 18g/L used in the previous SPARRO work. Alternatives to the Hydracell D10 pump are currently under investigation.

6.5. Conclusions on the experimental results to determine the effect of gypsum crystal morphology on membrane damage

Based on the experimental work that has been carried out, it is apparent that although there is evidence that gypsum crystal morphology does have an influence on the performance characteristics of cellulose acetate membranes, there is no conclusive evidence that the different morphologies actually damage the membranes.

Consequently, this finding places the focus, to a greater extent, on membrane fouling as the predominant membrane damaging mechanism as the reason for the failure in the SPARRO process. The fouling phenomenon is discussed later in this document.

7. Control of the desupersaturation reactor in the SPARRO Process

7.1. Reactor design

The 5 L lab-scale desupersaturation reactor was designed based on the literature review with the aim of achieving good solid-liquid suspension. Table 7 gives the specifications of the tank and impeller. Figure 26 shows the schematic of the tank and Figure 27 shows the details of the impeller. The tank diameter could not be set to the height of the liquid, due to availability of Perspex only in standard diameters. The highest possible ratio of liquid height to tank diameter of 0.773 was used.

Table 7: Tank geometry and impeller specifications

Number of baffles	4, 90° to each other
Tank diameter, T [m]	0.22
Baffle width	$0.1T$
Draft tube diameter	$0.5T$
Draft tube height	$0.5T$
Tank bottom geometry	Rounded bottom
Height of liquid	$0.773\ T$
Material of construction	Perspex
Impeller type	Axial, 4-pitched-blades
Pitch	45°
Impeller diameter, D	$0.33T$
Blade width	$0.2\ D$
Impeller clearance	$0.33\ H$
Material of construction	Stainless steel

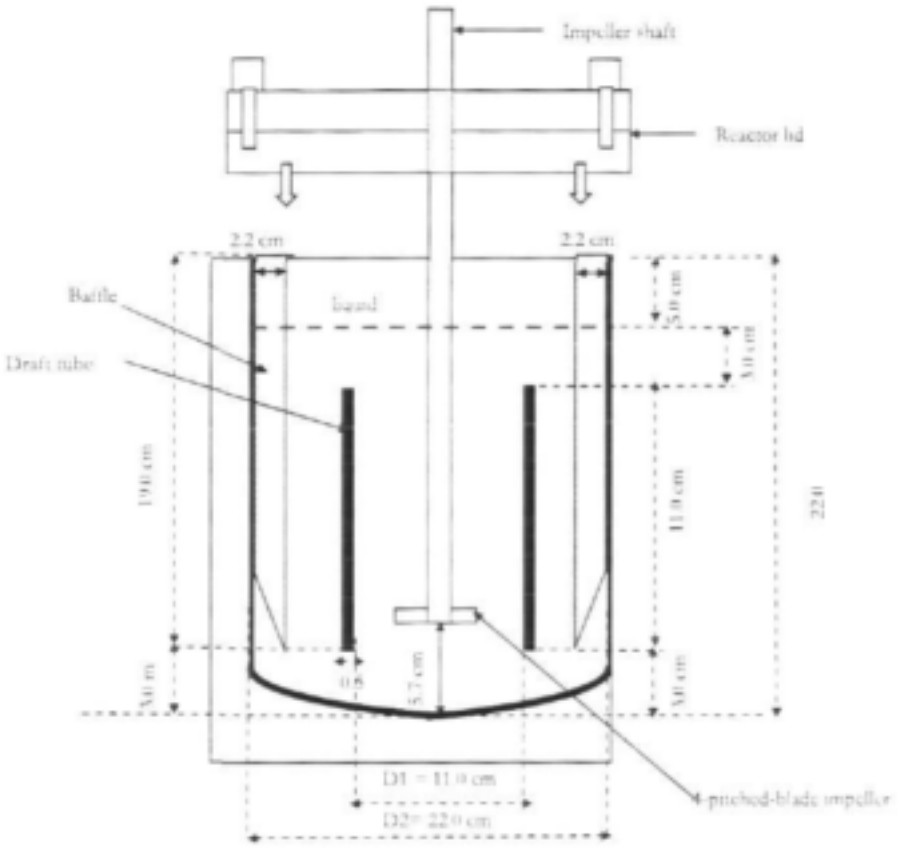

Figure 26: 5L lab-scale desupersaturation reactor

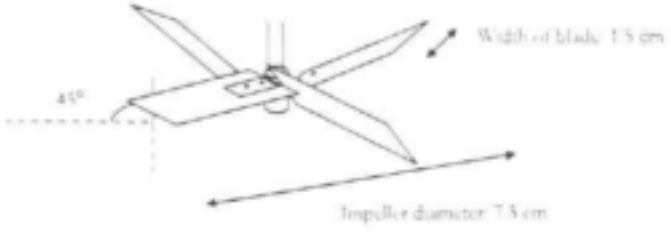

Figure 27: 4-pitched-blade impeller used in the experiments

7.2. Experimental design

Experiments aimed at fitting 1st and 2nd order models were carried out using a half-replicate 2^5 factorial design and axial point experiments respectively. Seed quantity, pH, stirrer speed and sulphate to calcium ratio were varied as continuous factors. Seed crystal morphology was kept as a discrete factor to compare the effects of using different seed morphologies.

Thus two half-replicates of 2^4 factorial design experiments were carried out for needle and plate-like crystals. The continuous factors were varied at levels given in Table 8.

Table 8: Levels of factors varied in experiments

Factor\Level	-2	-1	0	1	+2
SQ, Seed quantity [% by volume]	N/A	1	4	7	10
pH	1	4	7	10	N/A
N, Impeller speed [rpm]	N/A	300	500	700	900
SCR, Sulphate to calcium molar ratio	N/A	1	4	7	10

Some levels were not feasible due to negative values (e.g. –2 % by volume of seed crystals is impossible for –2 level) or because of physical constraints (e.g. impeller speed could not be set at 100 rpm for level –2, the minimum speed of the motor being 300 rpm). In these cases the +1 or –1 levels were used.
Table 9 lists the levels of the factors in the experiments carried out for the half-factorial 2^4 designs each for the needle and plate-like seed crystals.

Table 9: Half-replicate of 2^4 factorial design for needle and plate-like seed crystals

Experiment for needle	Experiment for plate	SQ	pH	N	SCR
A1	**B1**	1	1	1	1
A2	**B2**	-1	1	-1	1
A3	**B3**	0	0	0	0
A4	**B4**	-1	-1	1	1
A5	**B5**	0	0	0	0
A6	**B6**	-1	1	1	-1
A7	**B7**	0	0	0	0
A8	**B8**	1	1	-1	-1
A9	**B9**	1	-1	-1	1
A10	**B10**	0	0	0	0
A11	**B11**	-1	-1	-1	-1
A12	**B12**	1	-1	1	-1

To fit the second order model, axial point experiments were carried out. The levels at which the factors were varied in the experimental runs are given in Table 10.

Table 10: Axial point experimental runs for plate-like seed crystals

Experiment number	SQ	pH	N	SCR
C1	-1	0	0	0
C2	+2	0	0	0
C3	0	-2	0	0
C4	0	+1	0	0
C5	0	0	-1	0
C6	0	0	+2	0

C7	0	0	0	-1
C8	0	0	0	+2

To analyse the kinetics of the gypsum precipitating system, control experiments D1-D3 were carried out at the levels given in Table 11.

Table 11: Control experimental runs for plate-like seed crystals

Experiment number	SQ	pH	N	SCR
D1	-1	0	0	-1
D2	0	0	0	-1
D3	+1	0	0	-1

7.3. Experimental procedure

The experiments A1-A12, B1-B12, C1-C8 and D1-D3 were carried out in batch mode to investigate the effects of the factors independently without having a continuous stream coming into the reactor from the membrane module. The initial concentration of calcium ions was 0.03 M, a concentration that would typically occur in mine water.

The reactor was initially filled with 2.5 L of 0.06 M calcium chloride solution (prepared by dissolving high-purity anhydrous calcium chloride (Merck) in distilled water).

Needle-like or plate-like crystals were synthesized. The particle size distribution of the seed crystals was determined using a laser diffraction technique (Malvern Mastersizer, model MAM 5002). A small sample of the seeds was filtered through a Millipore 0.45µm filter using a vacuum pump. These crystals were dried for scanning electron microscopy. Preset quantities of seed crystals were transferred into the reactor.

The pH of the system was controlled by a pH controller (UCT custom-made), which was connected to an acid and base pump (UCT custom-made). pH readings were obtained and measured through a pH probe inserted in the reactor through an inlet provided on the reactor lid.

The position of the probe was outside the draft tube, in the annular region of the vessel. The probe was thus far from the acid and base inlet. 0.05 M NaOH and 0.05 M HCl solutions were used to increase and decrease the pH of the system. These solutions were prepared using analytical grade chemicals (Merck) and distilled water. The base and acid feed inlet in the reactor were located close to the impeller to ensure rapid dispersion.

The experiment was initiated by pumping (Masterflex peristaltic pump, model 7521-47) 2.5 L of sodium sulphate solution into the reactor at 9.5 ml/s. The feed point of sodium sulphate was kept close to the impeller to ensure good dispersion. The pH controller was activated and readings from a conductivity meter (Radiometer analytical, Ion check 30) were taken at 1-minute intervals. The conductivity probe was inserted in the reactor lid at a position far from the sodium sulphate feed point.

When the readings from the conductivity meter stabilised, samples were withdrawn from the sample port using a syringe. For all the experiments, the samples were taken from the same position in the reactor. The particle size distribution of the sample was measured using a laser diffraction technique (Malvern Mastersizer, model MAM 5002). Samples of crystals were filtered through a Millipore 0.45μm filter using a vacuum pump and left to dry for 96 hours for scanning electron microscopy.

7.4. Seed preparation

Preparation of needle-like seed crystals

Needle-like seed crystals were prepared by pumping (Masterflex peristaltic pump, model 7521-47) 0.08 M sodium sulphate solution at 9.5 ml/s into a 0.08 M calcium chloride solution. Analytical grade chemicals (Merck) and distilled water were used to prepare these reagents, which resulted in a weakly supersaturated solution (0.04 M, supersaturation ratio of 2.27) of calcium and sulphate ions. Therefore, a long induction time and large volumes of reagents were required to produce a small amount of seed crystals. A 15 L tank was used as the reacting vessel and a 4-pitched blade impeller, identical to that used in the desupersaturation reactor, was used to agitate the reagents at 500 rpm. Each batch of the 15 L preparation was left for 24 hours and yielded 200 ml of crystals (4% by volume in the 5L desupersaturation reactor). These crystals were filtered for use in the batch desupersaturation experiments.

Preparation of plate-like seed crystals

Plate-like seed crystals were prepared by direct addition of 0.4 M sodium sulphate solution to 0.4 M calcium chloride solution. These reagents resulted in a highly supersaturated solution (0.2 M, supersaturation ratio of 10.86) of calcium and sulphate ions. Therefore, a short induction time and small volumes of reagents had to be used to produce a large amount of seed crystals. A 250 ml beaker was used as the reacting vessel and a magnetic stirrer at 500 rpm was used for mixing the reactants. Each batch of the 250 ml preparation was agitated for 1 minute and yielded 25 ml of crystals (0.5% by volume in the 5L desupersaturation reactor). These crystals were filtered and used in the desupersaturation reactor. Dry samples of the seed crystals were ground and analysed by powder X-Ray Diffraction (Philips, model PW1050).

7.5. Responses and methods of analysis

The three responses that were measured were the time to reach equilibrium, % growth in the crystal size, and the crystal morphology.

Time to reach equilibrium

The conductivity meter provided an accurate and online measurement of the conductivity of the solution. When the conductivity meter readings were fully stabilised, the system was considered to have reached equilibrium. Reaction between the calcium and sulphate ions to form solid gypsum caused a decrease in the conductivity of the solution due to reduced ion concentration. The system volume and performance are affected when there is constant withdrawal of samples from the reactor whilst online measurements obviate the need to remove samples.

Percentage crystal growth

The mean particle size of the initial seed crystals, denoted by $D[4,3]_{seeds}$ and the mean particle size of crystals withdrawn from the equilibrium solution, denoted by $D[4,3]_{crystals\ at\ equilibrium}$ were used to calculate the percentage crystal growth:

$$\%\ crystal\ growth = \frac{(D[4,3])_{crystals\ at\ equilibrium} - (D[4,3])_{seedcrystal}}{(D[4,3])_{seedcrystal}} * (100) \qquad (14)$$

An average of three readings taken from the Malvern Mastersizer for each crystal sample was used for the mean particle size. Crystal samples were placed in an ultrasonic bath (ELA, model CP823) for 3-5 minutes at 25 °C at 90% power prior to size measurement to prevent particle agglomeration. Propanol was used as the medium as it acts as a good dispersant for gypsum particles. To minimise the amount of propanol, the 100 ml dispenser unit of the Malvern Mastersizer was used.

Percentage edges detection

The crystal morphology was expressed as the % edges detected over the digital image of the crystal sample. A scanning electron microscope (analytical, model S4440) was used to acquire these digital images. Dry samples of the crystals were mounted on stubs with carbon glue and coated with gold palladium alloy. The images were taken at a magnification of 1000x. The digital images were acquired using Matlab 6.5 with Image Processing Toolbox. The algorithm generated digital images of the edges detected in addition to the percentage edges detected. To record the error in measurement, 10 pictures of each sample were acquired and analysed by the image analysis and an average taken. A comprehensive description of the algorithm can be found in Seewoo (2003).

7.6. Hydrodynamic experiments

It was important to isolate mixing and reaction phenomena to determine the macromixing time scale of the 5L desupersaturation reactor. The reactor was initially filled with 5L of distilled water and the reactor lid was closed. The impeller was switched on at the required speed. 5 ml of 10 M sodium hydroxide solution was injected into the reactor at the sodium sulphate feed point location using a syringe and pH meter readings were taken every 10 seconds. The macromixing time was taken as the time at which the pH became steady. This procedure was repeated three times for different impeller speeds as listed in Table 12.

Table 12: Experiments for hydrodynamic studies

Experiment number	Impeller speed (rpm)
E1	300
E2	500
E3	700
E4	900
E5	1100

7.7. Aqueous chemistry modelling

OLI Systems Inc. (Stream Analyser 1.2) was used to model the gypsum precipitating system and investigate the effect of varying pH and sulphate to calcium ratios on the solubility of gypsum and for supersaturation ratio calculations.

7.8. Results and discussion

Seed material

The needle-like morphology (Figure 28) was generated under conditions of low supersaturation (supersaturation ratio 2.27) and was characterized by a lengthy induction time, prior to nucleation. The average length of the crystals was in the region of 100 μm. The plate-like seeds (Figure 29) resulted from conditions where the supersaturation ratio was higher, 10.86. This resulted in a significantly reduced induction time and a larger number of smaller (± 25 μm) crystals. A relatively larger specific surface area characterized the plate-like morphology.

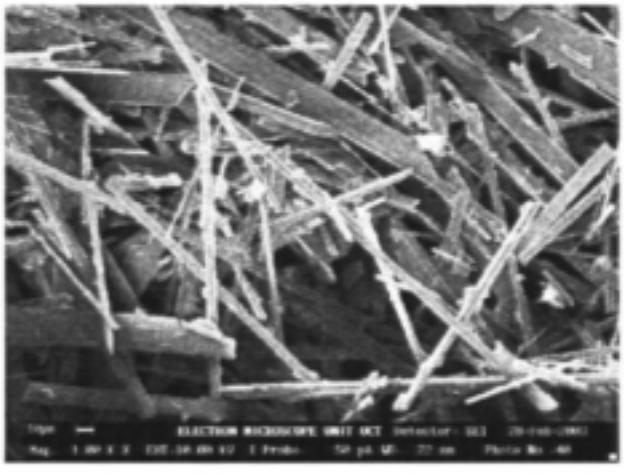

Figure 28: SEM image of needle-like seeds. 1 000x magnification. Scale bar 10 μm

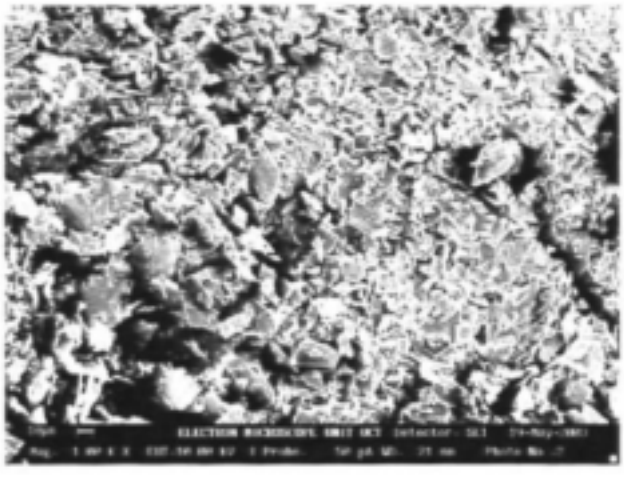

Figure 29: SEM image of plate-like seeds. 1 000x magnification. Scale bar 10 μm

Seed crystal purity

Representative samples of both morphologies were analysed by X-ray diffraction to determine the composition and purity of the material. The results (Figure 30) confirmed that the composition of both sets of samples was similar and identical to that of analytical grade gypsum.

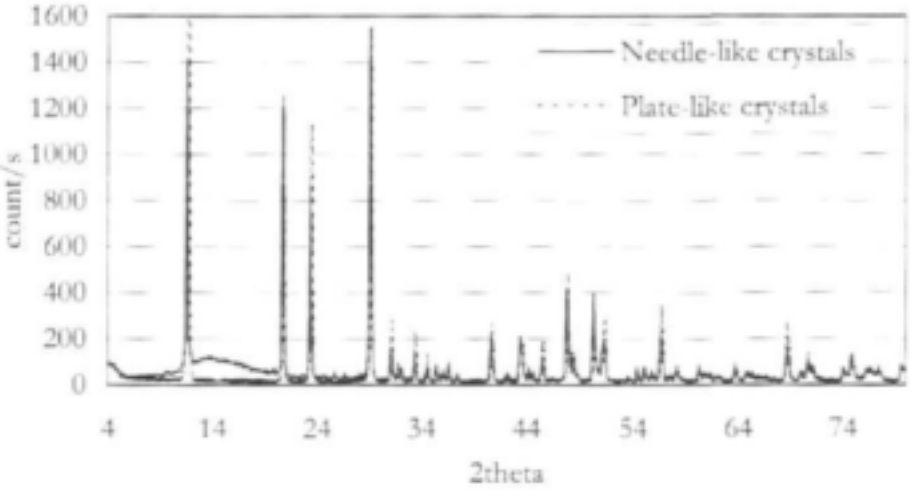

Figure 30: XRD traces comparing the composition and purity of needle- and plate-like seeds

Quantification of gypsum morphology

The processed images corresponding to Figure 28 and Figure 29 are shown in Figure 31 and Figure 32 respectively. The number of edges detected for the plate-like morphology is significantly greater than that for the needles.

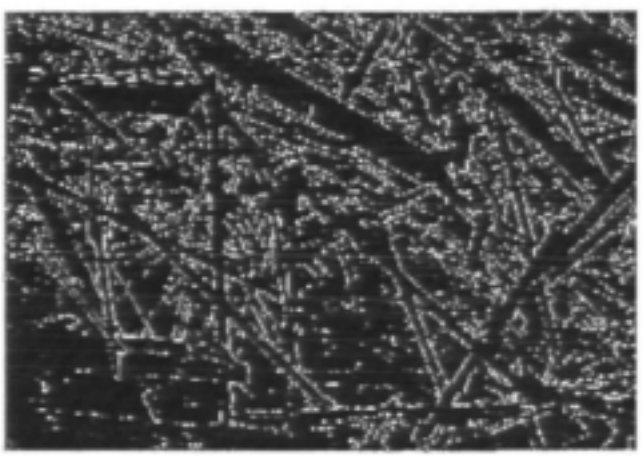

Figure 31: Processed image for needle-like seed crystals

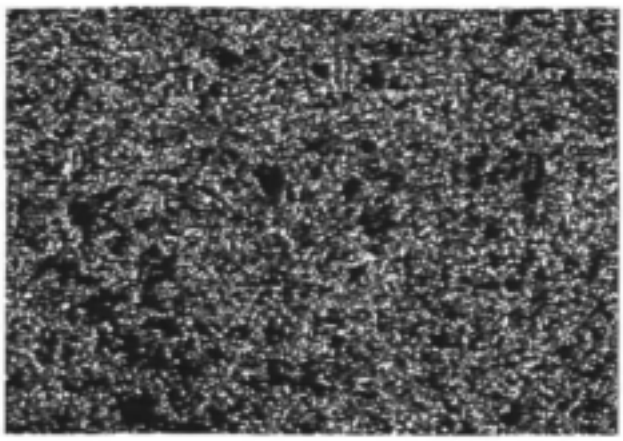

Figure 32: Processed image for plate-like seed crystals

A total of 30 images of each morphology were analysed. The results (Figure 33) show that there was no overlap between the edges detected for needle-like and plate-like crystals, confirming that two distinct morphologies have been identified and appropriately quantified.

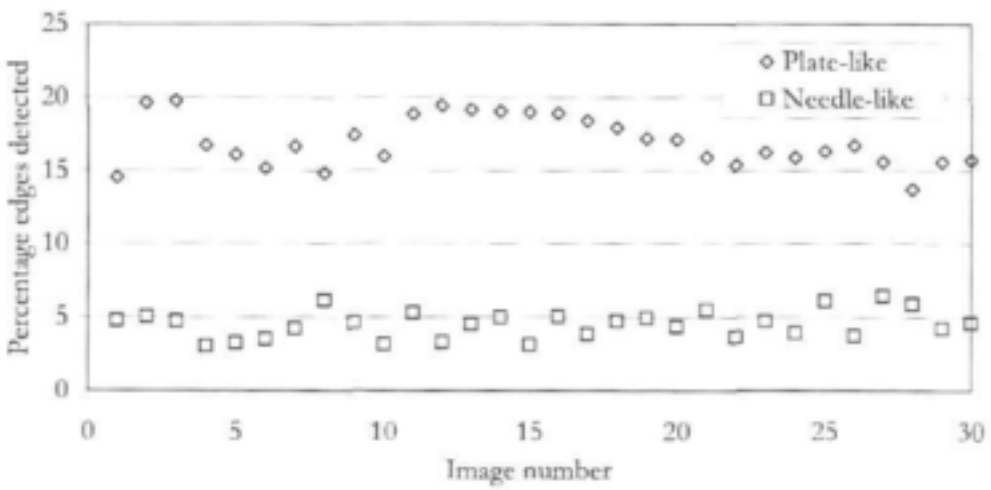

Figure 33: Percentage edges detected for needle- and plate-like seed crystals

Particle size distribution

The particle size distribution for gypsum seed crystals and those present in the reactor at equilibrium for a selected experimental run is shown in Figure 34. The mean particle size of

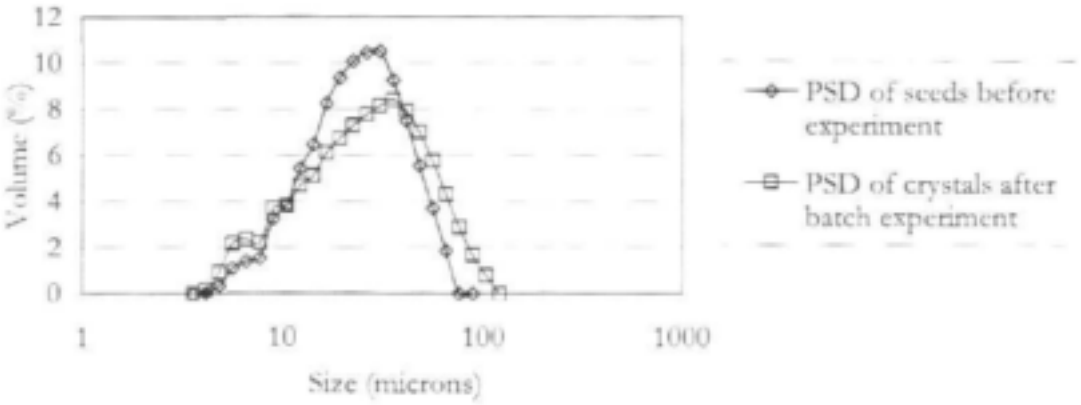

the seed crystals was 24.43 μm. At equilibrium, the mean size had increased to 28.94 μm. The increase in mean particle size is illustrated by a rightwards shift in the peak of the graph.

Figure 34: Particle size distribution of seed crystals and crystals present at equilibrium in experiment B5

This trend was consistent through all the experimental runs and suggests that the mechanism of desupersaturation is precipitation of gypsum onto existing seed material, resulting in an increase in seed size. The PSD data suggests that primary nucleation did not occur, which is consistent with the relatively low supersaturation conditions in the reactor. Under these conditions the primary nucleation rate would be significantly lower than the growth rate (Söhnel and Garside, 1992).

Effect of control variables on gypsum precipitation

- **Effect of sulphate to calcium ratio**

The stoichiometric ratio of sulphate to calcium ions in solution can affect the solubility of gypsum with an increase in the concentration of aqueous sulphate reducing the solubility of gypsum, due to the common ion effect. This effect can be modelled using thermodynamic based aqueous speciation software, such as OLI Systems Stream Analyser. Model data for the solubility of gypsum and corresponding supersaturation under the experimental conditions for a range of sulphate to calcium ratios is shown in Figure 35. This phenomenon was demonstrated experimentally by Liu and Nancollas (1970), who showed that an increase in sulphate ion concentration promoted gypsum crystal growth by reducing the solubility.

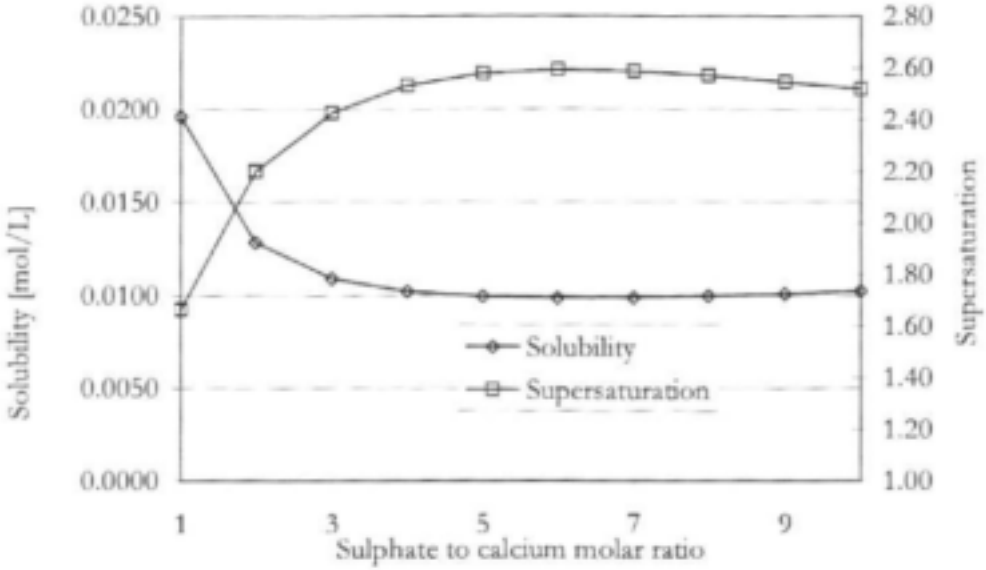

Figure 35: Effect of sulphate to calcium ratio on the solubility of gypsum, modelled using OLI Systems StreamAnalyser

* **Effect of pH**

Extremes of pH have an effect on the solubility of gypsum by affecting the speciation of the sulphate and calcium ions. Figure 36 illustrates this.

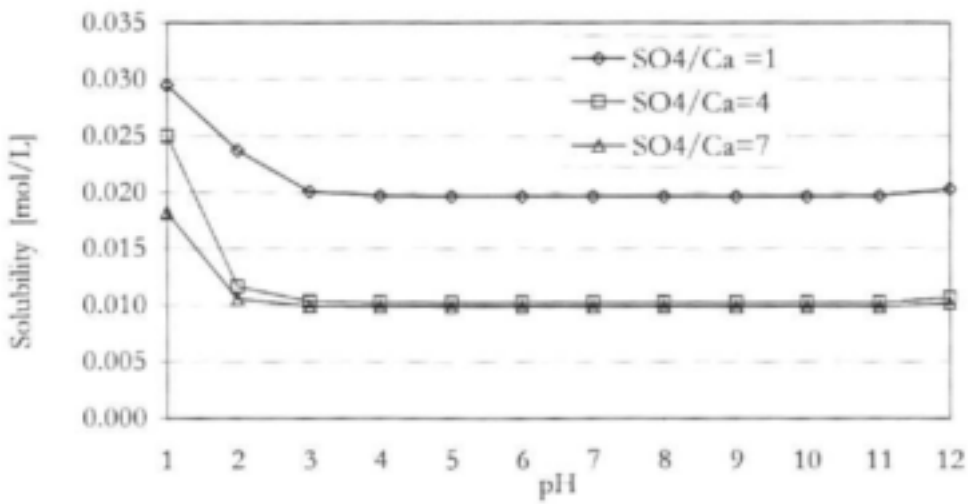

Figure 36: The effect of pH on gypsum solubility, modelled using OLI Systems, StreamAnalyser

Under acidic conditions, a significant portion of the sulphate ions may occur as the HSO_4^- species. As the concentration of H^+ ions increases, the sulphate species equilibrium is shifted toward the formation of HSO_4^-. This reduces the concentration of SO_4^{2-} ions in solution, increasing the solubility of gypsum. A stoichiometric excess of sulphate ions

mitigates this effect. Similarly, above pH 11, the calcium ions may undergo hydrolysis. The resulting $CaOH^+$ species reduces the Ca^{2+} ion concentration and increases gypsum solubility. These effects are shown in Figure 37.

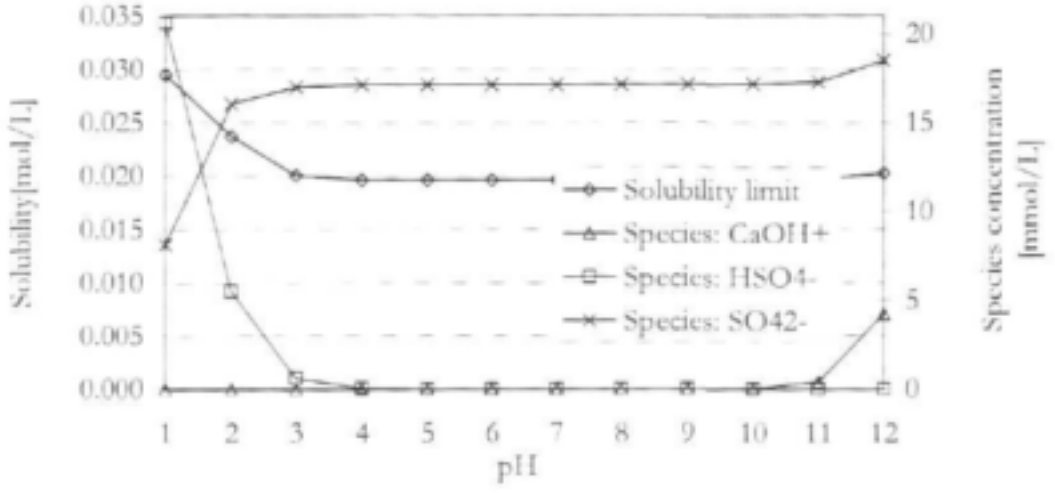

Figure 37: The effect of pH on Ca and SO_4 ion speciation, modelled using OLI Systems StreamAnalyser

* **Effect of seed morphology**

The morphology of the seed crystals had a significant effect on the kinetics of desupersaturation at low seed concentrations, where the time required to reach equilibrium in experiments seeded with needle-type crystals was up to three times longer than for the corresponding experiment using plates. This can be attributed to the higher specific surface area of the plates. At seed concentrations above 4% by volume this effect was not significant, suggesting the total surface area available was high enough not to be rate limiting.

The morphology of the seed crystals was shown to have a decisive influence on the seed morphology at equilibrium. Figure 38 and Figure 39 show the morphology of gypsum crystals harvested from the reactor at equilibrium for experiments A1 and B1 respectively, for which the operating conditions were identical and only the seed morphology differed.

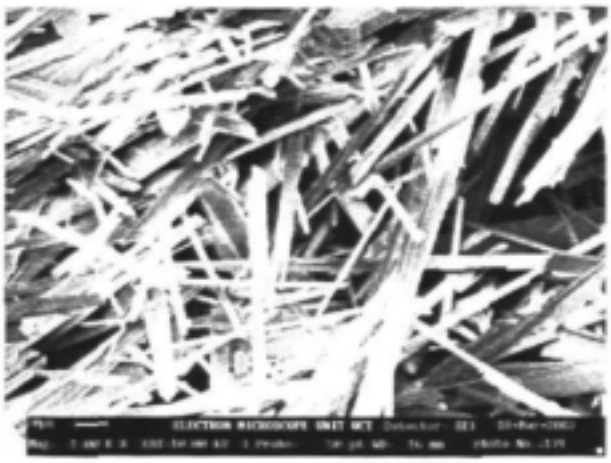

Figure 38: Crystals from experiment A1 at 1 000x magnification. Scale bar 20 µm

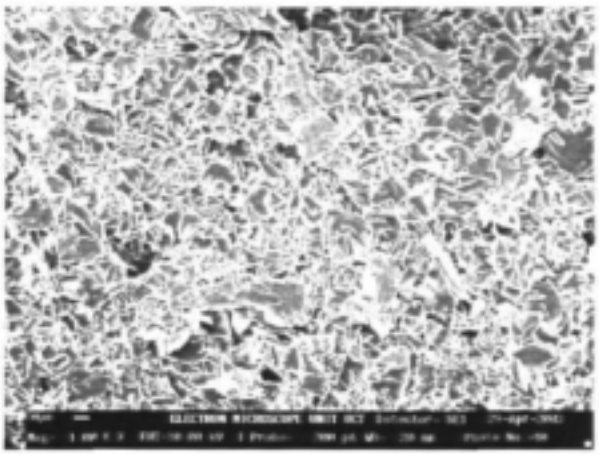

Figure 39: Crystals from experiment B1 at 1 000x magnification. Scale bar 20 µm

Image analysis of Figure 38 yielded a low percentage edges detected of 4.75 ± 1.02, while analysis of Figure 39 generated a higher percentage edges detected of 15.16 ± 2.06. This quantitative analysis also shows that the final crystal morphology remains similar to that of the seed crystals used in the process.

Based on the comparison of results presented above, the choice of an appropriate seed crystal has implications for the kinetics of gypsum precipitation and the final morphology of the crystals. When Juby (1994) developed the SPARRO process, insufficient emphasis was placed on the size and morphology of the seed crystals. An analysis of the seed particles showed that on average the particles were of similar shape and dimensions, roughly 100 µm in length and 20 µm wide. This description clearly fits the features of needle-like crystals. With precipitation occurring in the desupersaturation reactor, the needle-like morphology would have been maintained. Also, the use of needle-like seed crystals would have slowed the gypsum precipitation due to their lower specific surface area relative to plate-like crystals. These aspects were not explicitly examined in previous work.

- **Effect of seed quantity**

The seed quantity determined the available surface area upon which precipitation could occur and thus played a significant role in the rate of desupersaturation. In experiments D1-D3, which were conducted using plate-like seed crystals at 1, 4 and 7% by volume and a sulphate to calcium ratio of 1:1, equilibrium was reached in 152, 65 and 48 minutes respectively. In order to quantify the effect of seed quantity on reaction rate, the equation of Brandse et al. (1977) was modified to include conductivity, rather than solute concentration terms. The modified form is represented below:

$$-\frac{d\kappa}{dt} = P'\left(\kappa - \kappa^*\right)^n \qquad (15)$$

Where:
κ is the conductivity of the total ions present in the solution at time t
κ^* is the conductivity of the total ions present in the solution at equilibrium conditions
P' is a kinetic rate constant [cm(mS min)$^{-1}$ if n=2]
n is the order of the growth

The rate constant was determined by linearising the equation and determining the slope of the plot of $\frac{1}{\left(\kappa - \kappa^*\right)}$ versus t. The resulting plots are shown in Figure 40 and the rate constants are shown in Table 13 .

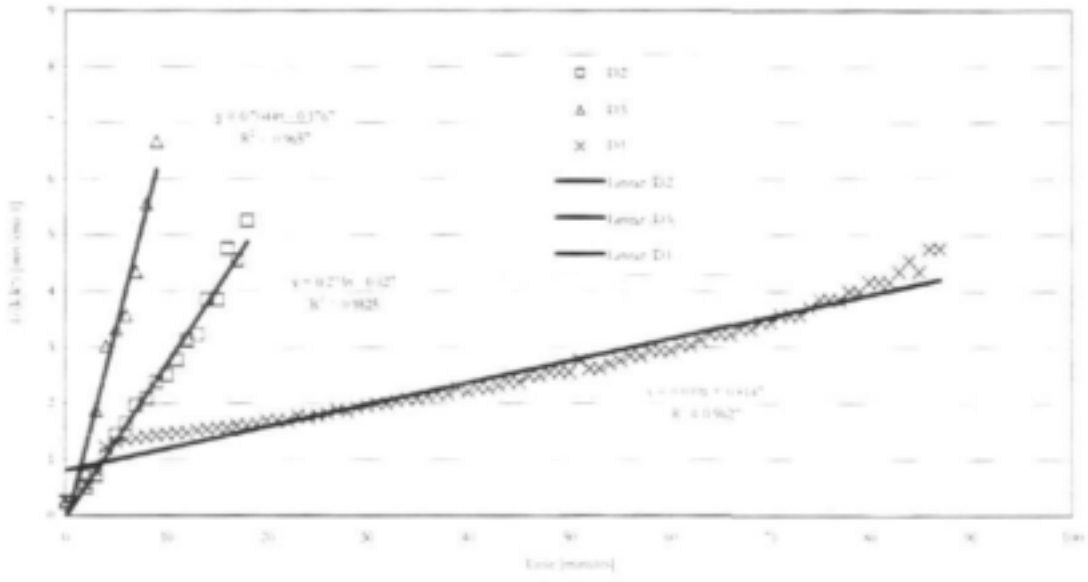

Figure 40: Determination of rate constants for experiments D1-3

Table 13: Rate constants obtained from experiments D1-D3

Experiment	Seed quantity [volume %]	Rate constant, P' [cm(mS min)$^{-1}$]
D1	1	0.039
D2	4	0.273
D3	7	0.704

The plots are linear for n = 2, confirming that the growth is second order. This result corresponds with those of Liu and Nancollas (1970, 1973, 1975), Brandse et al. (1977), Christofferson et al. (1982) and Çetin et al. (2001).

The seed quantity was also shown to have an effect on the morphology at equilibrium. As the seed concentration increased, the available surface area for precipitation increased, resulting in a smaller amount of precipitation on each seed and a smaller potential for a change in morphology. Table 14 shows the relationship between the amount of gypsum precipitated from solution and the quantity added as seeds.

Table 14: Comparison of mass of gypsum precipitated out of solution and mass of seed crystals

		1% by volume of seed crystals	4% by volume of seed crystals	7% by volume of seed crystals
Sulphate to calcium molar ratio	Mass of gypsum precipitated [g]	Mass of gypsum precipitated/Mass of seed crystals [%]	Mass of gypsum precipitated/Mass of seed crystals [%]	Mass of gypsum precipitated/Mass of seed crystals [%]
1	7.90	30.76	7.83	4.66
2	13.72	53.42	13.61	8.10
3	15.39	59.92	15.26	9.09
4	16.00	62.29	15.87	9.45
5	16.25	63.25	16.11	9.59
6	16.32	63.52	16.18	9.63
7	16.30	63.46	16.16	9.62
8	16.23	63.19	16.09	9.58
9	16.13	62.80	16.00	9.52
10	16	62.29	15.87	9.45

In previous research conducted on the SPARRO process, 1.76% by volume of seeds was added to the reactor (Juby, 1994). While this amount would be sufficient to result in precipitation on the seeds, the control of the morphology would be reduced.

* **Effect of agitation**

The macromixing times in the reactor at different impeller speeds was tested using the addition of NaOH as a tracer and measuring the time required for the pH to equilibrate. The data for macromixing time against agitation (Figure 41), represented by Reynolds number, are presented below.

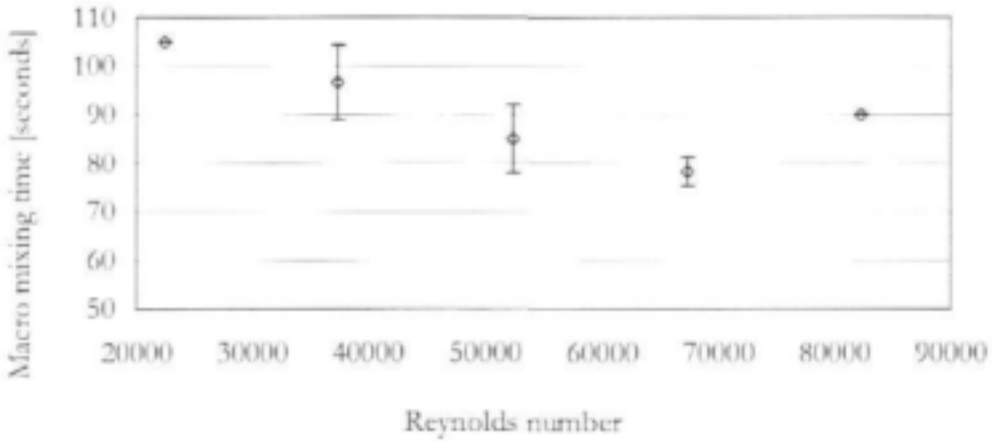

Figure 41: Effect of agitation on macromixing time

The Reynolds numbers obtained suggest that at all the values of impeller speeds the operating conditions were turbulent. From Figure 41 it can be seen that with an increase in the Reynolds number from 2.2×10^4 (300 rpm) to 6.7×10^4 (900 rpm) the macromixing time decreased from 105 to 78 seconds. As the Reynolds number increased, the turbulence in the reactor increased, which increased the circulation rate of bulk contents, decreasing the macromixing time. Beyond the Reynolds number 6.7×10^4 (900 rpm), the macromixing time increased. This increase could have been the result of excessively turbulent conditions within the reactor. Entrainment of air into the reactor was observed at Reynolds number 8.2×10^4 (1100 rpm). The air bubbles, which became entrained in the reactor, could also have compromised the pH readings.

The experimentally recorded macromixing times were, however, much larger than theoretical values calculated using the method of Baldyga and Bourne (1999). The difference in the macromixing times can be explained by time delays such as the pH probe response time as well as the position of the pH probe and the point of injection of the sodium hydroxide into the reactor. Nonetheless, the qualitative trend observed was consistent with that determined by theoretical calculation.

The micromixing times, calculated for the specific agitation conditions in the experimental program were all below 0.05 seconds. In all cases the micromixing times were significantly smaller than the reaction times. Therefore the reactor was essentially homogeneous and the precipitation reactor took place throughout the reactor (Söhnel and Garside, 1992).

An increase in Reynolds number was shown to increase the reaction rate and result in a smaller percentage increase in the mean crystal size (Figure 42).

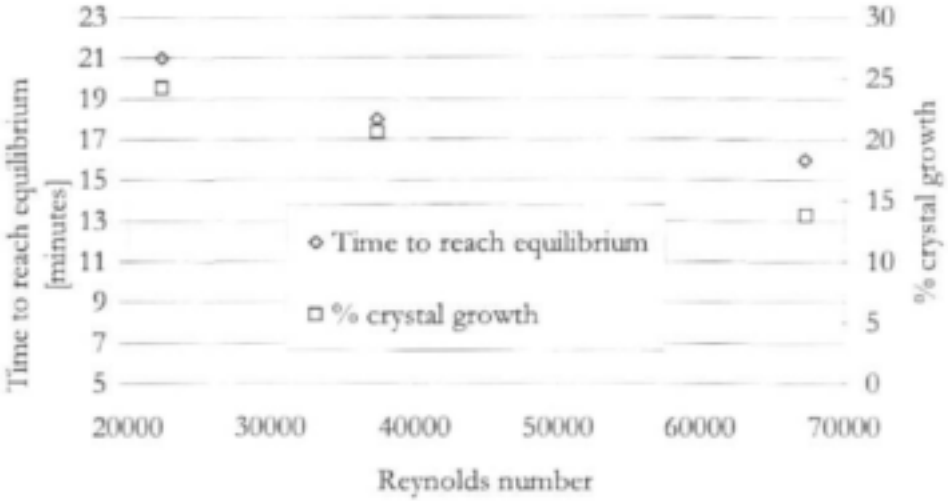

Figure 42: Effect of agitation on time to reach equilibrium and % crystal growth

These results can be discussed according to two hypotheses:

The first hypothesis is that there are to two zones that can be present in the stirred tank reactor (Pohorecki and Baldyga, 1988 and Chen *et al.*, 1996):

Zone 1: regions in the reactor where high supersaturation prevails
Zone 2: regions in the reactor where low supersaturation prevails

Regions described by zone 1 are a result of micromixing and lead to high nucleation rates. Regions described by zone 2 dilute any supersaturation in the bulk regions of the reactor and as a result, crystals growth overtakes nucleation. In the experimental results, an increase in impeller speed reduced the crystal growth. This suggests that with an increase in impeller speed, the area of influence of zone 1 increases (Pohorecki and Baldyga, 1988 and Chen *et al.*, 1996). The reaction spreads in regions of zone 1. With higher supersaturation prevailing, the driving force for precipitation increases and equilibrium is reached faster. Also, with higher supersaturation profiles, primary nuclei are formed, which reduces the percentage crystal growth.

It can be questioned whether the model of the reactor presented by Chen *et al.* (1996) and Baldyga and Pohorecki (1988) can be applied to this case of gypsum precipitation. The following are key differences between the system studied by Pohorecki and Baldyga (1988) and Chen *et al.* (1996) and the system investigated in this research project:

- $BaSO_4$ was the precipitated product, which Pohorecki and Baldyga (1988) and Chen et al. (1996) studied. In this project gypsum is under investigation. The solubility product of $BaSO_4$ and gypsum are 1.1 E-10 and 2.4 E-5 respectively. This means that at the same concentration, the supersaturation of $BaSO_4$ would be significantly higher than that of gypsum

- Pohorecki and Baldyga (1988) and Chen et al. (1996) studied the spontaneous precipitation of $BaSO_4$. In the case with the system under investigation, seeding was used. Seeding preferentially induces precipitation by crystal growth (Bremere et al., 1999).

Over and above the differences presented above, there following are points that provide evidence that nucleation was unimportant in the gypsum seeded system that was studied and that growth of seed crystals was the mechanism by which solutions precipitated:

- Nucleation processes in gypsum seeded precipitation were found to be unimportant by Christoffersen et al., 1982. They investigated gypsum precipitation from solutions at supersaturation ratios of 1.03 to 2. In the current system, the maximum supersaturation ratio was 2.6.
- There exists a critical supersaturation ratio of 4, below which the nucleation rate is measurably slow (Mullin, 2001). The supersaturation in the system under investigation was below the critical supersaturation ratio.
- The mass of gypsum precipitated from solution in the experiments compared to the mass of the seed crystals corresponded to the percentage growth of crystals calculated.
- The significant difference between micromixing time and reaction time suggests that the reactor is homogeneous.

The second hypothesis is particle attrition. As the Reynolds number increased in experiments C5, B3 and C6, particle attrition could have occurred. This could have increased the number of particles as well as increasing the available surface area, therefore reducing the time to equilibrium, assuming a growth dominated system.

Weighing the hypotheses presented in an attempt to explain the effect of mixing suggests that there is more evidence that nucleation was not the cause of decrease in percentage crystal growth and time to reach equilibrium in experiments C5, B3 and C6. However, it cannot be confirmed that no nucleation was occurring. This presents a gap in this research and further work involving crystal number counting can be carried out. In order to prove the attrition hypothesis, further experiments can be carried out. These can involve investigating the effect of Reynolds number on the particle size of gypsum seed crystals. These experiments should be carried out in a saturated solution of gypsum to prevent crystal growth and to allow independent study of the influence of shear rate.

Statistical analysis and response surfaces

The aims of the statistical analysis of the experimental data were:

- To identify the factors that have the greatest impact on seeded gypsum precipitation,
- To locate the ideal operating conditions for the desupersaturation reactor.

The results database was analysed by the STATISTICA software package. The following sections give the first order models fitted for the responses when needle-like and plate seed crystals were used (experiments A1-A12 and B1-B12) and the second order models fitted for the responses when plate-like seed crystals were used (experiments C1-C8). Table 15 and Table 16 show the notation and units of the responses and factors used in the models.

Table 15: Notation and units of responses used in models

Response	Notation	Unit
Time to reach equilibrium	T	Minutes
Percentage crystal growth	% growth	-
Percentage edge detected	% edge	-

Table 16: Notation and units of factors used in the models

Factor	Notation	Unit
Seed quantity	SQ	% volume
PH	PH	-
Stirrer speed	N	rpm
Sulphate to calcium ratio	SCR	-

* **First order models**

Effect of process parameters on time to reach equilibrium

The effects of the process parameters on the time to reach equilibrium using needle-like and plate-like seed crystals are given by the best-fit models in Table 17 and Table 18 respectively. The standard errors (SE) and the p-values are also given.

Table 17: 1st order model for time to reach equilibrium using needle-like seed crystals

T =	286.6250	-25.1667(SQ)	-0.66667(pH)	-0.06125(N)	-14.4167(SCR)
SE	64.33	5.38	5.38	0.08	5.38
P-values	0.0030	0.0023	0.90	0.47	0.031

Table 18: 1st order model time to reach equilibrium using plate-like seed crystals

T =	179.3750	-13.9167(SQ)	-1.0833(pH)	-0.03125(N)	-12.250(SCR)
SE	53.76	4.49	4.49	0.067	4.49
P-values	0.013	0.017	0.82	0.66	0.029

The models in Table 17 and Table 18 account for 80.9% and 71.2 % of the variation in the time to reach equilibrium respectively. The p-values identify seed quantity and sulphate to calcium ratio as the most significant factors affecting the time required to reach equilibrium in both of the first order models.

Effect of process parameters on percentage crystal growth

The effects of the process parameters on the percentage crystal growth using needle-like and plate-like seed crystals are given by the best-fit models presented in Table 19 and Table 20 respectively.

Table 19: 1st order model for % crystal growth using needle-like seed crystals

% growth =	38.0990	- 6.3871(SQ)	- 1.04958(pH)	- 0.01497(N)	- 1.46542(SCR)
SE	13.55	1.13	1.13	0.02	1.13
P-values	0.0261	0.0008	0.3849	0.41	0.24

Table 20: 1st order model % crystal growth using plate-like seed crystals

% growth =	72.1827	- 5.7071(SQ)	- 1.0579(pH)	- 0.012056(N)	- 1.9096(SQR)
SE	11.87	0.99	0.99	0.015	0.096
P-values	0.0005	0.0007	0.3215	0.4443	0.096

The models in Table 19 and Table 20 account for 83.4 % and 84.7 % of the variation in the percentage crystal growth respectively. Seed quantity is the most significant factor affecting percentage crystal growth in both the models as can be seen by the corresponding p-values.

Effect of process parameters on gypsum crystal morphology

The effects of the process parameters on gypsum crystal morphology as measured by % edges detected using needle-like and plate-like seed crystals are given by the best-fit models presented in Table 21 and Table 22 respectively.

Table 21: 1st order model for % edges detected using needle-like seed crystals

% edge =	2.99750	+ 0.11750(SQ)	- 0.00250(pH)	- 0.00390(N)	- 0.26500(SCR)
SE	13.55	1.13	1.13	0.02	1.13
P-values	0.0261	0.0008	0.3849	0.41	0.24

Table 22: 1st order model for % edges detected using plate-like seed crystals

% edge =	6.5388	+ 0.43750(SQ)	- 0.04417(pH)	- 0.000538(N)	+ 0.4741(SCR)
SE	2.52	0.21	0.21	0.0032	0.21
P-values	0.036	0.077	0.84	0.87	0.06

The models in Table 21 and Table 22 account for 64.7 % and 57.4% of the variation in the % edges detected respectively. The p-values show that seed quantity has the greatest influence on the % edges detected in both the models.

The R^2 values for all the first order models were relatively low. These gave grounds to fit second order models using plate-like seed crystals. The analysis of variance indicated that the responses of time to reach equilibrium, percentage growth and percentage edge detected were curvilinear within the experimental region. This meant that second order models could be fitted and the critical region where a minimum, maximum or saddle point occurred could be located.

Comparison of first order models using needle and plate-like crystals

A test was carried out to find whether a single first order model is appropriate for both needles and plate-like seed crystals. The discrete factors (plate-like and needle-like seed crystals) were included in the model and given values 0 and 1 respectively. From the analyses of variances for each of the response variables, it was evident that different models needed to be fitted for plate and needle-like seed crystals. The p-values for the t-statistics were all less than 0.05, confirming that the responses obtained using plate and needle-like seed crystals were significantly different. The seed crystal morphology affects both the kinetics of gypsum precipitation and the final crystal morphology. Kinetics are faster when plate-like seed crystals are used because they provide a larger surface area for gypsum precipitation as compared to when the needle-like seed crystals are used. Maintenance of the plate-like morphology is possible by seeding with plate-like seed crystals.

* Second order models for plate-like seed crystals

Second order model for time to reach equilibrium

Table 23 summarises the second order model fitted to the response of time to reach equilibrium.

Table 23: 2^{nd} order model for T using plate-like seed crystals

Parameter	Parameter estimate	Standard error	p-value
Intercept	331.573820	31.934095	0
SQ	-47.375184	5.627490	0
SCR	-39.026347	3.635723	0
pH	-8.824160	4.503383	0.0857
N	-0.202148	0.085261	0.0452
$(SQ)^2$	2.218246	0.324207	0.0001
(SQ)(SCR)	2.388889	0.418687	0.0005
$(SCR)^2$	2.101967	0.324207	0.0002
(SQ)(pH)	0.666667	0.418687	0.15
$(pH)^2$	0.414628	0.324207	0.2368
(SQ)(N)	0.003333	0.006280	0.61
$(N)^2$	0.000152	0.000072947	0.0707

This best-fit model accounts for 97.84 % of the variation in the time to reach equilibrium. The critical point is a minimum, which occurs at a seed quantity of 6.33% by volume, a sulphate to calcium ratio of 5.68, a pH of 5.54 and a Reynolds number of 4.5×10^4 (595 rpm). According to the model, at the critical point, it takes –14 minutes for the reacting gypsum system to reach equilibrium. Even though this result is physically impossible, the model provides the operating region at which the time to reach equilibrium can be minimised. The seed quantity and sulphate to calcium ratios are the most significant contributors in the second order model. Keeping the least significant factors, pH and impeller speed, constant at 7 and 500 rpm (Reynolds number of 3.7×10^4), Figure 43 shows the 3-d surface of the model. The corresponding contour plot is shown in Figure 44 and the corresponding response values are shown on the contours.

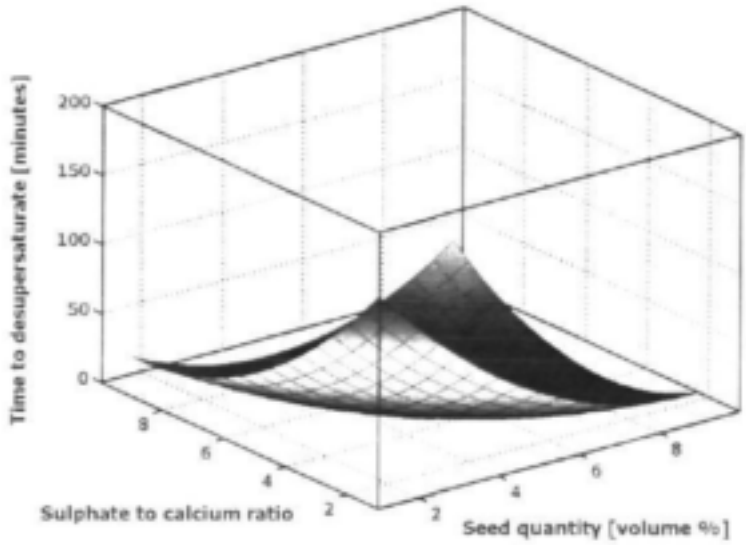

Figure 43: 3-D surface plot for time to reach equilibrium, factors pH and N constant

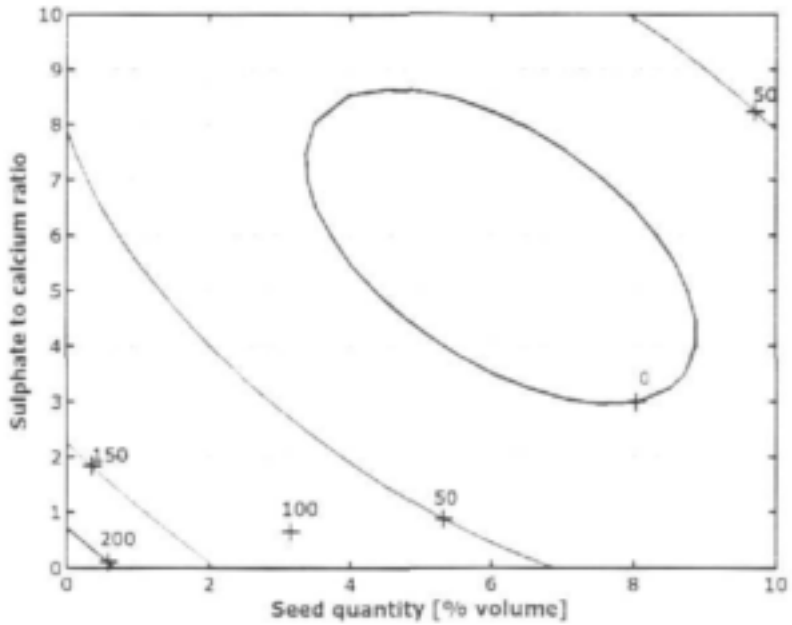

Figure 44: Contour plot for time to reach equilibrium, factors pH and N constant

Second order model for percentage crystal growth

Table 24 summarises the second order model fitted to the response of percentage crystal growth.

Table 24: 2nd order model for % growth using plate-like seed crystals

Parameter	Parameter estimate	Standard error	p-value
Intercept	102.006560	25.062063	0.0036
SQ	-14.763188	4.416486	0.0102
SCR	-6.189756	2.853336	0.0619
pH	-3.583593	3.534281	0.3403
N	-0.037686	0.066914	0.5887
$(SQ)^2$	0.558443	0.254440	0.0595
(SQ)(SCR)	0.388472	0.328588	0.2711
$(SCR)^2$	0.361350	0.254440	0.1933
(SQ)(pH)	0.187361	0.328588	0.5842
$(pH)^2$	0.195226	0.254440	0.4650
(SQ)(N)	0.004881	0.004929	0.3510
$(N)^2$	0.000003676	0.000057249	0.9504

This best-fit model accounts for 84.99 % of the variation in the percentage crystal growth. A critical point, a minimum, occurs at a seed quantity of 8.06 % by volume, a sulphate to calcium ratio of 4.54, a pH of 5.39 and Reynolds number of 3.7×10^4 (496 rpm). A 9.08 % increase in crystal growth can be achieved at that critical minimum point. Seed quantity and sulphate to calcium ratio are the most significant contributors in the second order model. Keeping the least insignificant factors, pH and impeller speed, constant at 7 and 500 rpm (Reynolds number of 3.7×10^4). Figure 45 and Figure 46 show the surface of the model and the corresponding contour plot respectively.

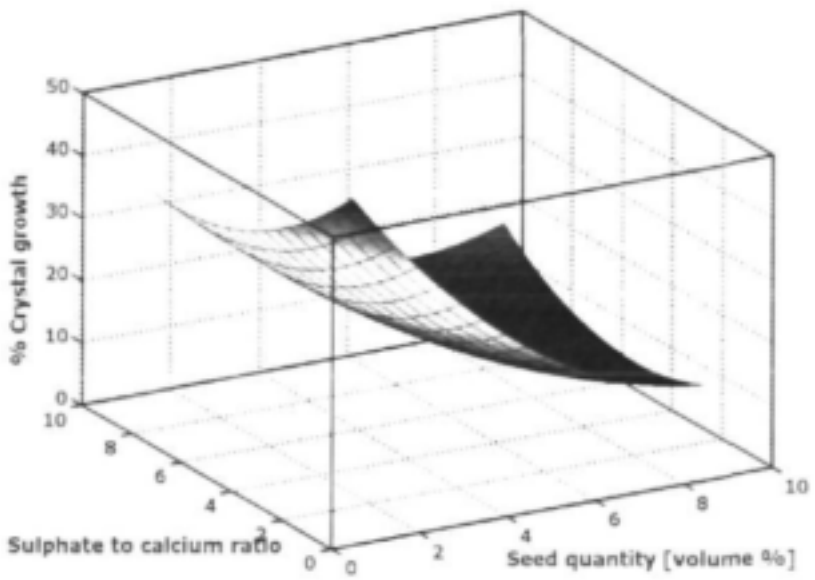

Figure 45: 3-D surface plot for % crystal growth, factors pH and N constant

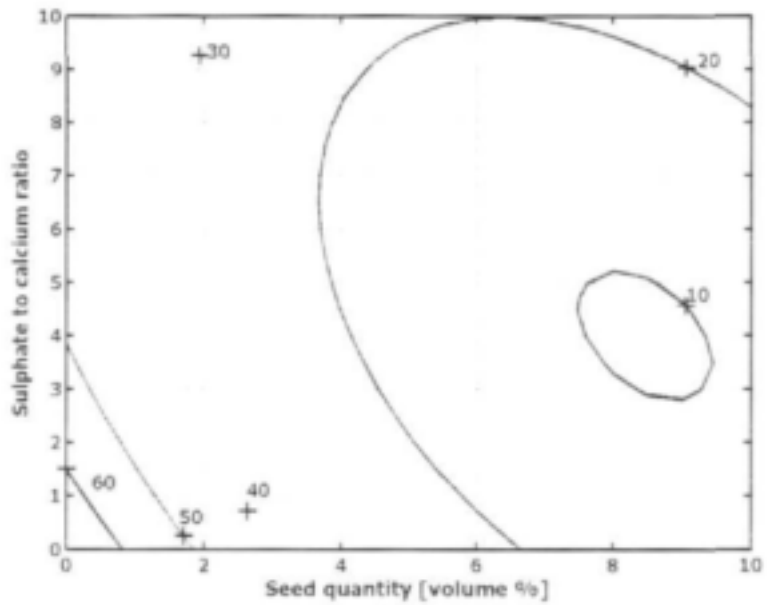

Figure 46: Contour plot for % crystal growth, factors pH and N constant

Second order model for percentage edges detected

Table 25 summarises the second order model fitted to the response of percentage edges detected.

Table 25: 2nd order model for % edge detected using plate-like seed crystals

Parameter	Parameter estimate	Standard error	p-value
Intercept	9.791481	4.30667	0.0526
SQ	-1.364805	0.0758930	0.1098
SCR	-0.536837	0.490318	0.3054
pH	0.2536860	0.607331	0.6871
N	-0.000184	0.011498	0.9877
$(SQ)^2$	0.085918	0.043723	0.0850
(SQ)(SCR)	0.169167	0.056465	0.0172
$(SCR)^2$	0.049975	0.043723	0.2861
(SQ)(pH)	0.001944	0.056465	0.9734
$(pH)^2$	-0.020064	0.043723	0.6585
(SQ)(N)	0.001137	0.000847	0.2161
$(N)^2$	-0.000002680	0.000009838	0.7922

This best fit model accounts for 89.06 % of the variation in the percentage edges detected. The interaction parameter between the seed quantity and the sulphate to calcium ratio, AD, significantly affects the crystal morphology. The higher the seed quantity and sulphate to calcium ratio, the higher is the percentage edges detected. The critical point for the percentage edges detected lies outside the experimental region. Figure 47 and Figure 48 show the 3-d surface and corresponding contour plot at pH 7 and impeller speed of 500 rpm (Reynolds number of 3.7×10^4). A ridge analysis reveals that a percentage edge detected as high as 22% can be achieved by using 9% by volume of seed crystals, 8.23 sulphate to calcium ratio, a pH of 5.5 and a Reynolds number of 4.8×10^4 (644 rpm).

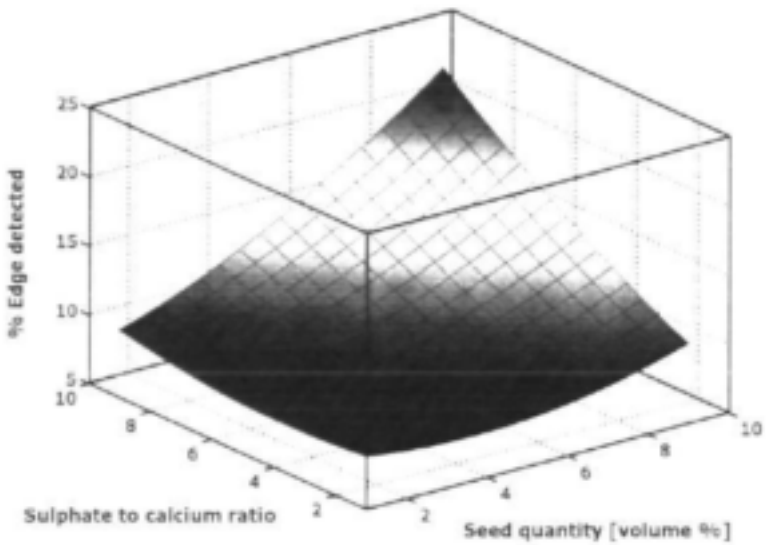

Figure 47: 3-D surface plot for % edges detected, factors pH and N constant

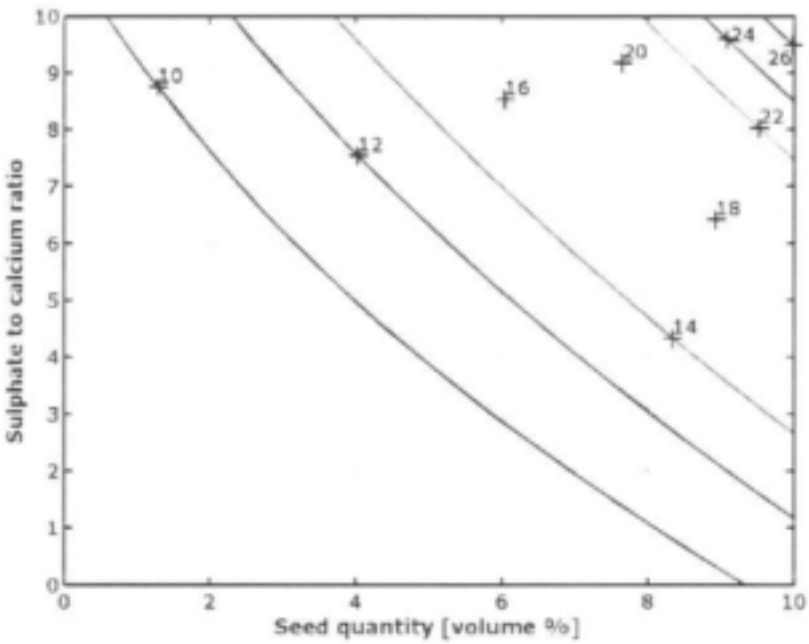

Figure 48: Contour plot for % edges detected, factors pH and N constant

7.9. Location of the ideal operating conditions for the desupersaturation reactor

It is one of the aims of the project to define the operating conditions for the operation of the desupersaturation reactor. The operating conditions need to achieve:

- A minimum time required for gypsum solution to reach equilibrium,
- A minimum crystal growth to occur,
- A maximum possible percentage edges detected - to maintain the morphology of the crystal to the plate-like morphology.

The second order models obtained when plate-like seed crystals were used show that regions of minimum for the time to reach equilibrium and percentage crystal growth were located. By fixing the pH and impeller speeds at 7 and a Reynolds number of 3.7 x 10^4 (500 rpm), the contour plots illustrated in Figure 49 and Figure 50 were generated. Figure 49 shows the two contour plots superimposed. The region shaded in green is the region where the two responses are at a minimum. This area defines the operating region, which can simultaneously satisfy a minimum for time to reach equilibrium, and percentage crystal growth.

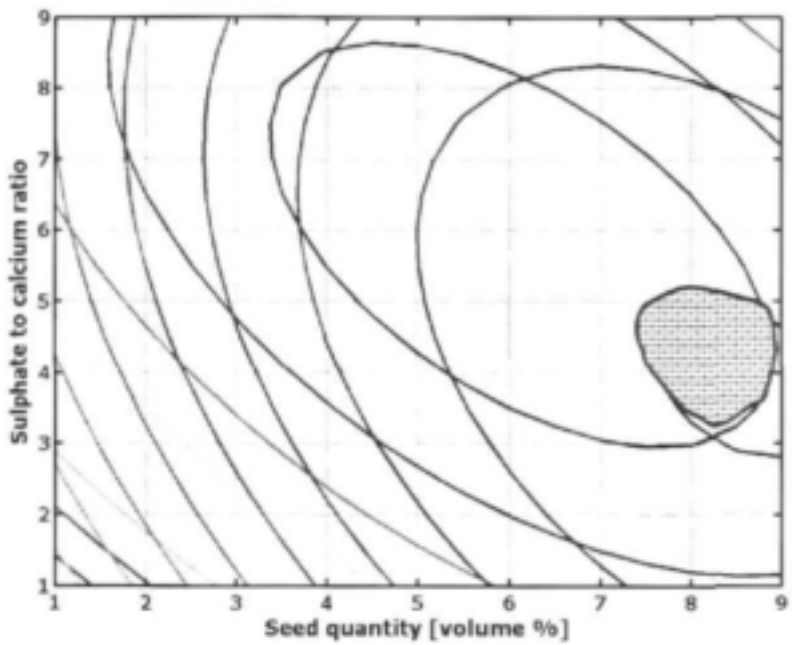

Figure 49: Contour plots of time to reach equilibrium and % crystal growth overlapped

The third criterion that needs to be achieved in the SPARRO desupersaturation reactor is the crystal morphology to be kept as plate-like as possible. The higher the percentage edges detected, the more plate-like the crystal is. It was beyond the scope of this project to carry out test on the membrane modules. An investigation into the effect of crystal morphology on membrane damage in the SPARRO process can establish the size and morphology of gypsum crystals, which cause least damage to the membranes. The percentage edges detected for those particular crystals can then used to determine the ideal operating conditions for the desupersaturation reactor. The contour plot for the percentage edges detected is overlapped on the Figure 49 to give Figure 50.

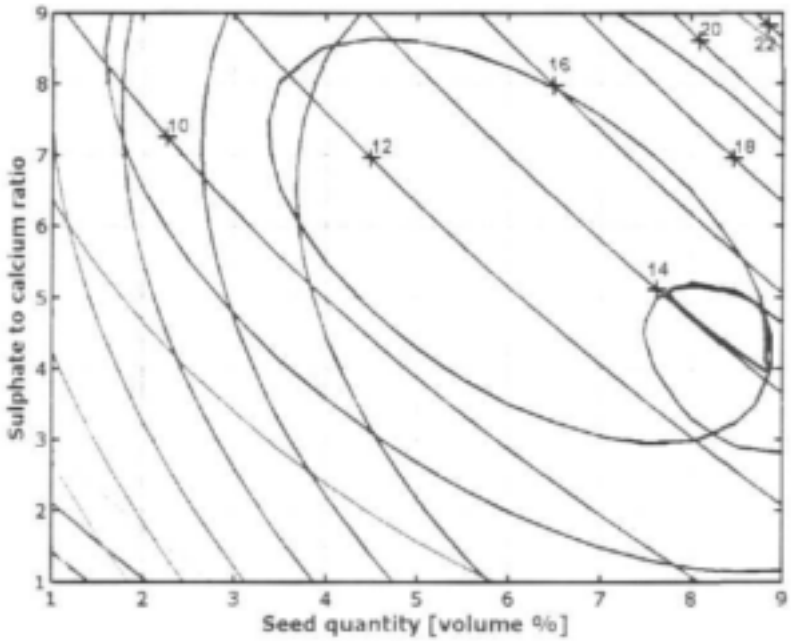

Figure 50: All three contour plots overlapped

The red lines represent the percentage edges detected and the corresponding values are shown on the contours. From Figure 50, it is possible to read off the required percentage edges detected and thus isolate the feasible operating region. For example, for operating conditions that yield a percentage edge detected of above 12%, the shaded green area on Figure 49 would meet all criteria required for the reactor. For 14% edges detected, then the area shaded in purple as shown in Figure 50 would define the operating conditions required to meet all the criteria of the reactor. For 16% edges detected, then all the criteria will not be met. In that case, a trade-off between the three responses and the levels of the factors would need to be carried out.

8. CRITICAL OPERATING PARAMETERS FOR THE SPARRO SYSTEM

The final aim of the research project is achieved by integrating the crystallisation studies with the membrane studies and developing a design basis and understanding for the SPARRO process.

8.1. Aqueous Chemistry Analysis

One of the recommendations arising from the second Steering Committee meeting was to carry out some aqueous chemistry modelling in order to ascertain how the complex aqueous chemistry of the real waters under consideration would affect the findings of this research which, of necessity, is based on synthetic waters. The scope of this work was the particular crystallisation focus brought to bear on the membrane process, and not a crystallisation study in its own right. Thus, the contribution here rests in the integration of the membrane studies with the crystallisation studies and, for this reason, the crystallisation studies focussed on the issues of crystal morphology in pure solution.

Although crystallisation of pure salts from the scaling point of view has been extensively studied, the complexity of the scaling process has mostly restricted scaling research to a single salt precipitant. However, it is known (Sheikholeslami, 2003) that co-precipitating salts exert interactive effects, with or without common ions. These effects include solubility effects, rate effects, crystal structure and strength effects and also dynamic effects.

The available thermodynamic predictive models and software only consider the speciation effects and the ionic strength effect and there is not yet any universally applicable thermodynamic method to incorporate the effect of other precipitating salts. Recent work (Yu et al, 2002; Chong and Sheikholeslami, 2002; Sheikholeslami, 2003) has demonstrated that the co-existence of salts does affect both the kinetics and thermodynamics of the system. However, it must be emphasised that each of these studies was carried out on a very specific and relatively simple water system; usually a single salt with one additional species in solution. In depth thermodynamic and kinetic scaling studies on the complex waters relevant to this work have not yet, to the authors' knowledge, been carried out.

Nonetheless, some positive information can be gleaned from the available thermodynamic predictive models on the effect of chemical speciation and ionic strength on the scaling potential of pure compared to complex waters. In this study, both of these effects were examined.

Effect of water recovery on supersaturation (scaling potential)

A selection of mine waters were analysed to investigate the effect of water recovery on the scaling potential of the specific mine water under consideration. In precipitation systems, the most critical parameter is the supersaturation whereas, for the operation of the SPARRO system, the most critical parameter is the water recovery. These two parameters were related in the models. The aqueous chemistry software used was OLI Stream Analyser (OLI Systems, 2003) and the following mine waters were modelled:

Table 26: Selected mine waters for aqueous chemistry modelling

(Analyses below give the full extent of information available)

Source Parameter	Units	Seewoo (2003) Orange Free State Mine	Inap (2003) Secunda coal mine water: pre RO	Juby (1994) Grootvlei phase 1	Juby (1994) Grootvlei phase 2	Inap (2003) Copper mine water
pH		6.5	7.1	6.17	4.76	2.8
TDS	Mg/L	3800	4092	2219	9410	4860
Cl	mg Cl/L	1400	313	55	196	10
SO_4	mg SO_4/L	1050	2125	1237	5560	3350
Na	mg Na/L	1000	920	272	745	42
Ca	mg Ca/L	330	176	309	468	266
Mg	mg Mg/L	30		33	635	153
Fe	mg Fe/L		0.3	0.3	0.61	
Mn	mg Mn/L			0.2	35.8	87
K	mg K/L					8
Al	mg Al/l			0.6	17.6	220
Cu	mg Cu/L					114
Zn	mg Zn/L			0.2	6.5	143
Ni	mg Ni/L			0.4	24.9	

The graph in Figure 51 shows the effect of water recovery (%) on the supersaturation for five different mine waters (note the log scale on the ordinate), including the Grootvlei water from phases 1 and 2. The precipitation line is marked on the graph as the level above which scale formation will occur. A striking feature of the graph is the significant degree of supersaturation of aluminium hydroxide for the Grootvlei waters, indicating that $Al(OH)_3$ precipitation will occur across the entire range of water recoveries. The high level of $Al(OH)_3$ in the system also explains the fouling effect of $Al(OH)_3$ on the membranes experienced by Juby (1994), when attempting to run the SPARRO system using the Grootvlei phase 1 and 2 waters.

Another interesting feature of Figure 51 is the fact that the Grootvlei phase 2 water enters the treatment system already supersaturated with respect to gypsum. This can be seen by the $CaSO_4.2H_2O$ line being above the precipitation line over the entire range of water recoveries.

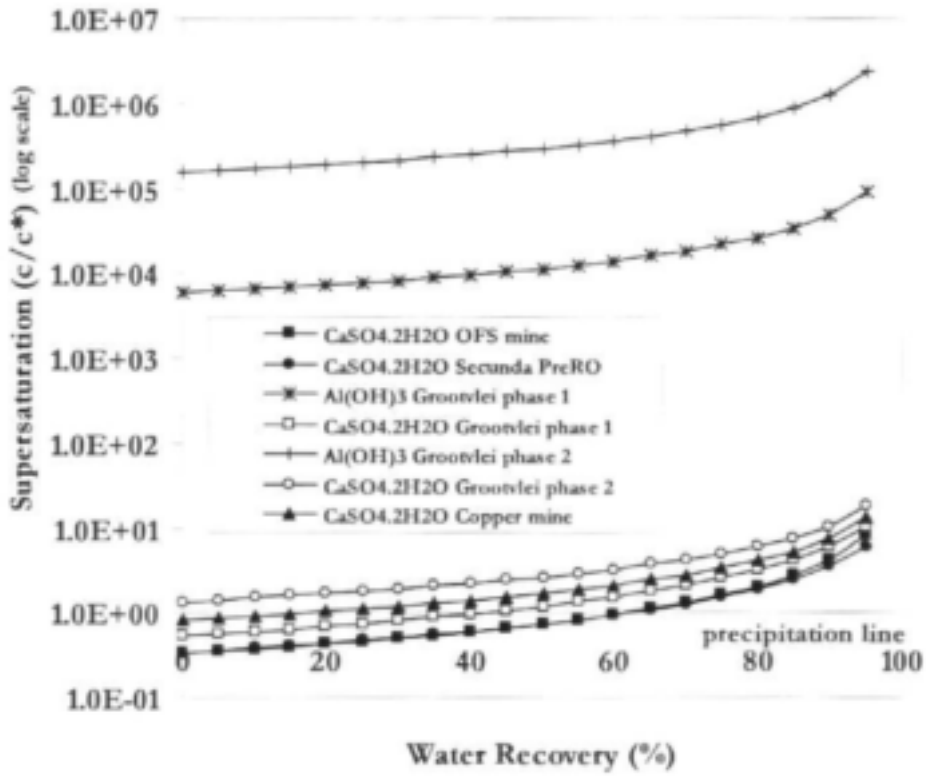

Figure 51: Effect of water recovery on supersaturation and aqueous chemistry for five mine waters. Includes Aluminium for the Grootvlei waters and has a log scale on the ordinate.

The next graph, Figure 52, shows the same information (no log scale on the ordinate), but with the Aluminium excluded. Here it can be seen that supersaturations of greater than 1 are generated as the expected water recovery increases to above 60%, and the onset of precipitation occurs in the system. For water recoveries of 90% and higher, extremely high supersaturations are generated in the concentrate.

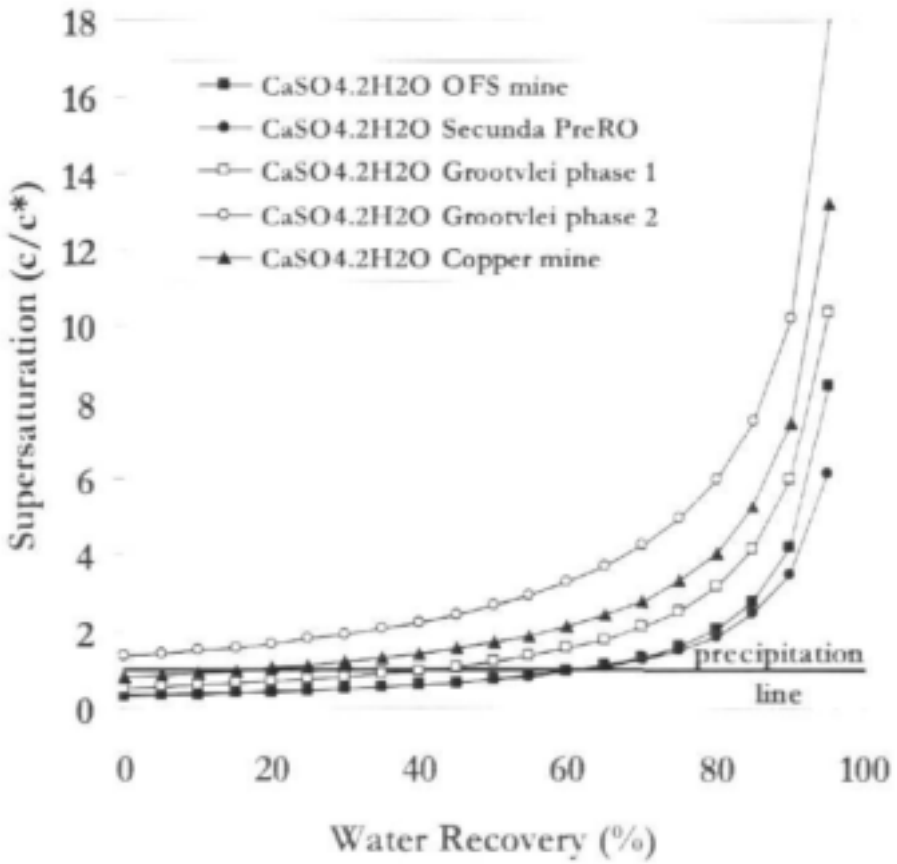

Figure 52: Effect of water recovery on supersaturation and aqueous chemistry for 5 mine waters. Aluminium hydroxide removed from the Grootvlei waters and no log scale on the ordinate

Effect of water composition on gypsum solubility

The second investigation focussed on the effect of the complex aqueous chemistry on the precipitation potential of gypsum. It should be borne in mind that even one other salt dissolved into solution with calcium sulphate will significantly complicate the aqueous chemistry. The currently available thermodynamic models only take into account the speciation and ionic strength effects, and these have been investigated here. The aqueous chemistry software used was OLI Stream Analyser (OLI Systems, 2003) and the following waters were analysed:

13. The pure laboratory water used in the investigation ($H_2O + CaCl_2 + Na_2SO_4$)
14. Secunda coal mine water (analysis given in Table 26)
15. Grootvlei phase 2 water. (analysis given in Table 26)

The graph in Figure 53 demonstrates the effect of chemical speciation on gypsum solubility. The pure water system exhibits the theoretically expected solubility curve from the calculation carried out using the solubility product of gypsum in the absence of any other aqueous ionic species besides the counter ions. For the Secunda coal mine water, the solubility of gypsum is decreased because of the presence of other ionic species – specifically sulphate species in solution. For the Grootvlei phase 2 water, the solubility curve intersects with the ordinate because the water is already saturated with respect to calcium sulphate i.e. no amount of reduction of the sulphate ion in the form of sodium sulphate will allow more calcium sulphate to dissolve in solution, since it is already at the maximum.

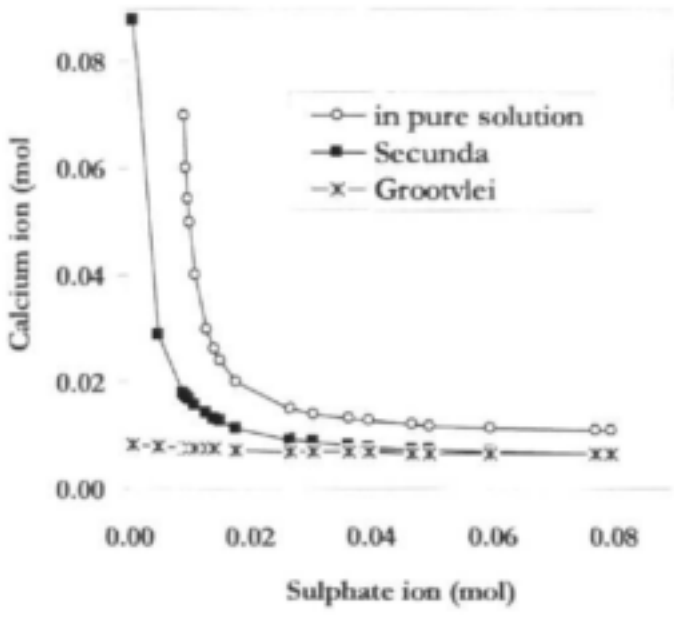

Figure 53: Effect of water composition on gypsum solubility

Effect of ionic strength on gypsum solubility

Figure 54 illustrates the effect of ionic strength on the solubility of gypsum in pure solution. The result is somewhat counter intuitive; as it is clear that the solubility of gypsum increases in the presence of KCl. The effect is more pronounced at higher ionic strengths. The reason for the increase in solubility is due to the ionic interactions between the solute ions and the solvent ions. As the gypsum dissolves in solution, the calcium and sulphate ions interact with the other ions in solution, which allows for more gypsum dissolution because only free ions enter into the expression for the solubility product equilibrium constant. From a mathematical point of view, in higher ionic strength solutions, activity coefficients for calcium and sulphate become smaller, and hence the concentrations must be larger to maintain a constant solubility product at equilibrium (Willey, 2004).

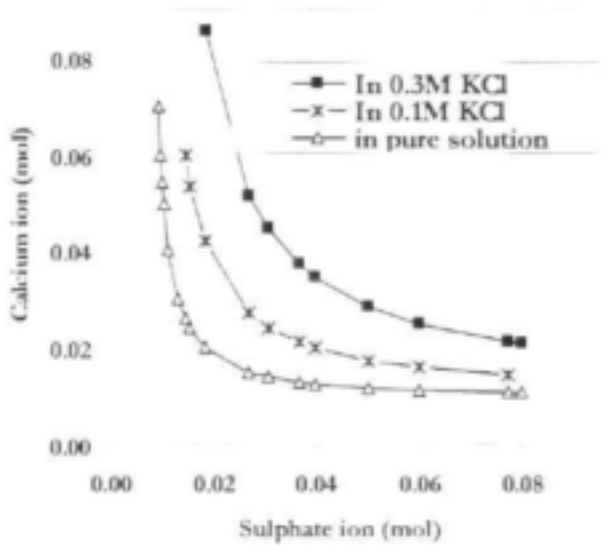

Figure 54: Effect of ionic strength on gypsum solubility in pure solution

The implications of these two modelling exercises for the complex mine waters under consideration are contradictory:

16. On the basis of water composition, the scaling potential of the complex mine waters is **increased** compared to the pure solution;
17. On the basis of ionic strength, the scaling potential of the complex mine waters is **decreased** compared to the pure solution;

More detailed modelling and experimental studies would need to be carried out in order to establish the net effects of these two counteractive effects.

8.2. Control of Crystal Morphology

From the Sparro Membrane Test Rig (SMTR) mini-plant studies and the Directed Slurry Spraying Technique (DSST), it is clear that, besides the aqueous chemistry, control of crystal morphology is essential in order to minimise membrane damage in the SPARRO process. In this process, there are three parameters that can be used control the morphology:

- Supersaturation to control nucleation
- Supersaturation to control growth
- Seed volume to control morphology

Supersaturation and nucleation

Precipitation within the membrane modules can only occur in three ways: by nucleation as a new particle, on existing seed crystals and on the surface of the membrane (Juby, 1994). The first form of precipitation is homogeneous nucleation and is only possible in the bulk fluid if the supersaturation, or driving force, is sufficiently high. The second form is heterogeneous nucleation, or nucleation onto a foreign surface, and requires a lower supersaturation. The last form of precipitation is secondary nucleation, or nucleation onto the crystallising material itself, and this requires the lowest supersaturation of all. This is illustrated below in Figure 55, where:

- region 4 represents homogeneous nucleation (in the bulk);
- region 3 represents heterogeneous nucleation (onto the membrane);
- region 2 represents secondary nucleation (on the seeds);

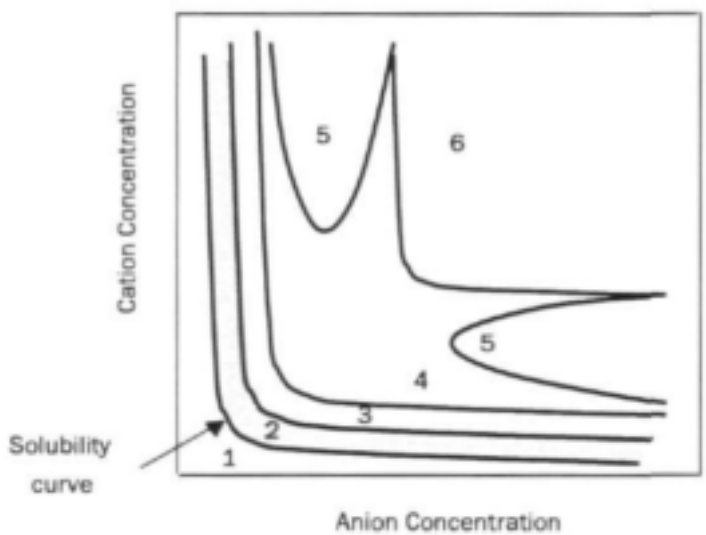

Figure 55: Effect of supersaturation on form of nucleation (Gosele & Kind, 1991)

From a nucleation control point of view, it is clear that anything more than a slightly supersaturated solution must be avoided and that the supersaturation of the solution must be maintained at the supersaturation levels of region 2 but not regions 3 and 4.

Juby was under the misapprehension that providing enough seed surface area alone would be sufficient to prevent heterogeneous nucleation. But nucleation is primarily a function of supersaturation. If the supersaturation is too high, heterogeneous nucleation (i.e. in the membrane) will occur no matter how much seed surface area is available. The control parameter to prevent heterogeneous nucleation in the membrane is the supersaturation, which, in this application, is controlled by controlling the water recovery.

Supersaturation and growth

Crystal morphology is usually controlled by crystal growth. The needle-like gypsum morphology is a feature of a growth dominated region, which occurs under conditions of relatively low supersaturation (approximately <2), whilst the platelet morphology dominates at regions of higher supersaturation (approximately >2). Note that these values are highly specific to particular systems, as they are dependent on aqueous chemistry speciation, ionic strength as well as the presence of other ionic species.

From the point of view of control of the SPARRO process, the needle-like morphology is more likely to cause membrane damage and thus slightly supersaturated solutions should be avoided.

Unfortunately, the recommendations with respect to nucleation (avoid high supersaturation) and growth (avoid low supersaturation) are conflicting. However, there is another control variable that can be used to manipulate the crystal characteristics in the SPARRO system.

Seed volume and morphology

If the supersaturation is controlled at low enough levels to prevent heterogeneous nucleation in the membrane, then the morphology of the crystals must be controlled by another parameter which, in this case, is the seed volume.

Juby (1994) calculated the surface area of the membrane to be 0.32m/L of tubular membrane volume. With a seed concentration of less than 2g/L, the seed area and membrane area were more or less equivalent. At a seed concentration of approximately 18g/L (the concentration used in Juby's work), the estimated seed surface area was approximately 10 times that of the membrane. This translates into a seed volume % of 0.8 vol% . In order to maintain this seed volume concentration in the membrane, the desupersaturation reactor had to be maintained at a seed volume concentration of 41g/L i.e. 1.76 vol% .

However, this calculation is based on the misunderstanding that the only requirement is for the surface area of the seeds to be greater than the surface area of the membrane. Since the presence of the seeds alone cannot control the supersaturation, but can only provide templates for growth, their function is to absorb the supersaturation as rapidly as possible and thus control morphology. If the seeds absorb the supersaturation sufficiently rapidly, then a secondary benefit will be that it will not reach sufficiently high levels such that heterogeneous nucleation occurs in the membrane. This is due to the kinetic effect of providing a large surface area to consume the supersaturation. However, it should be emphasised that this is a consequence of the system operating conditions and not a driving force in its own right.

For this purpose, a variable amount of seeds depending on the supersaturation is required. If the supersaturation is low, the quantity of seeds must be increased to avoid the formation of needles. If the supersaturation is high (but lower than that for heterogeneous nucleation), the quantity of seeds can be reduced accordingly. The design chart in Figure 56 below illustrates the concept for a pure calcium sulphate solution containing sodium and chloride as counter ions.

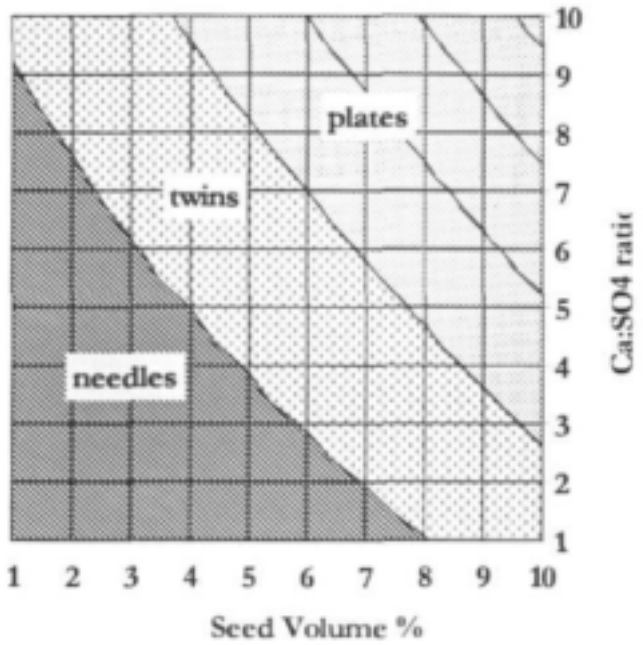

Figure 56: Design chart for seed volume and sulphate: calcium ratio related to morphology

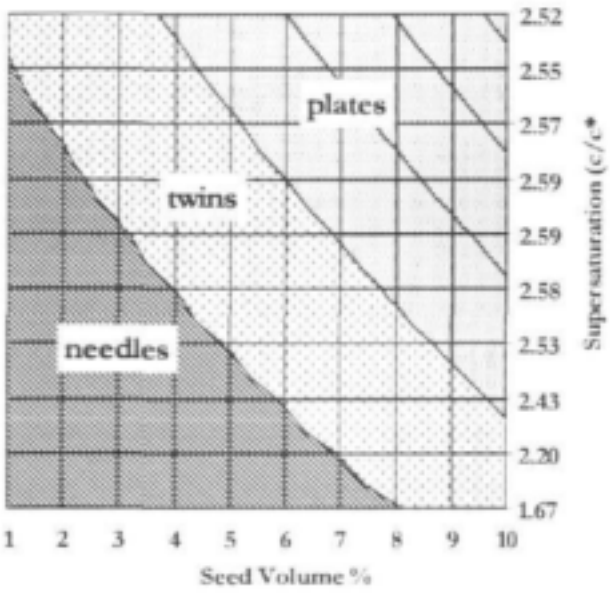

Figure 57: Design chart for seed volume and supersaturation related to morphology

In summary, the conclusions that can be drawn from this aspect of the work are:

- For the selected mine waters, a water recovery of approximately 60% is achievable before the supersaturation increases to the scaling level. The Grootvlei phase 1 and phase 2 waters are both supersaturated with respect to $Al(OH)_3$ which is responsible for the fouling mentioned in Juby's report. The Grootvlei phase 2 water is also supersaturated with respect to $CaSO_4.2H_2O$;

The implications of the two modelling exercises for the complex mine waters under consideration are contradictory:

- On the basis of water composition, the scaling potential of the complex mine waters is increased compared to the pure solution;
- On the basis of ionic strength, the scaling potential of the complex mine waters is decreased compared to the pure solution;

More detailed modelling and experimental studies would need to be carried out in order to establish the net result of these two counteractive effects.

From the Sparro Membrane Test Rig (SMTR) mini-plant studies and the Directed Slurry Spraying Technique (DSST), it is clear that, besides the aqueous chemistry, control of crystal morphology is essential in order to minimise membrane damage in the SPARRO process. In this process, there are three parameters that can be used control the morphology:

* Supersaturation to control nucleation

    * Supersaturation to control growth
    * Seed volume to control morphology

- If heterogeneous nucleation in the membrane is to be avoided, the supersaturation must be controlled. This can be manipulated by adjusting the water recovery.
- If sufficient seeds are provided, the morphology of the gypsum crystals can be controlled to the platelet shape, **even in regions where the needle morphology is dominant**. Thus, the membrane damaging needle-like morphology can be avoided.

Model design charts that relate seed volume and supersaturation or sulphate: calcium ratios to gypsum morphology in pure solutions have been developed.

9. CONCLUSIONS

Considerable success has been attained in addressing the central question of this research project, which is: **To what extent do the crystallisation parameters affect membrane damage in the SPARRO system?**

The crystallisation aspects of the process have been thoroughly investigated and an extensive understanding of gypsum crystal behaviour developed. Design specifications relating to the crystallisation parameters of the system and control of the desupersaturation reactor have been developed based on the critical operating parameters for the SPARRO system.

The conclusions from the crystallisation aspects of the work are as follows:

- Rate of consumption of supersaturation is significantly increased by the use of seeds as a source of secondary nucleation;
- Needle-like seeds were produced under conditions of low supersaturation and were characterised by a long induction time;
- Plate-like seeds were formed at high supersaturation, with a significantly reduced induction period;
- Digital image processing could be used to quantitatively distinguish between gypsum morphologies;
- XRD analysis showed similar traces for all morphologies and analytical grade gypsum;
- Sulphate to calcium ratio and pH extremes affected the solubility of gypsum and thus the rate of desupersaturation by the common ion effect and influence on the speciation of SO_4^{2-} and Ca^{2+};
- Seed morphology controlled the morphology at equilibrium under the batch conditions investigated;
- At low seed concentrations, the plate-like seeds significantly reduced desupersaturation times due to higher specific surface area;
- The kinetic rate constant for growth was affected by seed quantity (due to available surface area);
- Increased agitation reduced desupersaturation time and relative increase of seed size, suggesting attrition under conditions of high turbulence;
- Statistical analysis confirmed that, of the four factors tested, the seed quantity had the most significant effect on all three response variables;
- A set of operating conditions were identified to minimise desupersaturation time, while still maintaining a plate-like precipitate morphology

The conclusions from the membrane aspects of the work are as follows:

Gypsum morphology does have the potential to play a significant role in influencing membrane performance based on the SMTR experimentation. In particular, for intermittent SMTR operation, the needle type morphology had a greater detrimental effect on both salt rejection and membrane flux, with the system taking up to 8 hours to return to the optimal performance levels subsequent to a shut down. In continuous operational mode, with a seeds concentration of 2 g/L, evidence shows that the needle morphology shows a greater degree of variability in salt rejection and membrane flux when compared to the platelets.

However, for continuous operation, with a seeds concentration of 14 g/L, over an operational time of 160 hours, there was no significant variation in the salt rejection over time, when compared to the results of the standard salt test. Thus, the evidence is inconclusive in terms of being able to categorically declare that gypsum crystal morphology does have a significant influence on membrane damage in the SPARRO process.

Based on the slurry spraying technique, the damage caused by the needle type morphology was significantly more pronounced when compared to that of the platelet type morphology. This compliments the results obtained using the SMTR in that crystal morphology has the potential to cause membrane damage.

The implications of this work are that, if the platelet morphology of the crystals in the SPARRO process is maintained, membrane damage is expected to be reduced.

Critical operating parameters for the SPARRO system.

Aqueous chemistry modelling was carried out using predictive thermodynamic software in order to ascertain how the complex aqueous chemistry of the real waters under consideration would affect the findings of this research which, of necessity, is based on synthetic waters. It was found that:

- For the selected mine waters, a water recovery of approximately 60% is achievable before the supersaturation increases to the scaling level. The Grootvlei phase 1 and phase 2 waters are both supersaturated with respect to $Al(OH)_3$ which is responsible for the fouling mentioned in Juby's report. The Grootvlei phase 2 water is also supersaturated with respect to $CaSO_4.2H_2O$;

The two modelling exercises for the complex mine waters under consideration give rise to opposing conclusions:

- On the basis of water composition, the scaling potential of the complex mine waters is increased compared to the pure solution;
- On the basis of ionic strength, the scaling potential of the complex mine waters is decreased compared to the pure solution;

More detailed modelling and experimental studies would need to be carried out in order to establish the net result of these two counteractive effects.

From the Sparro Membrane Test Rig (SMTR) mini-plant studies and the Directed Slurry Spraying Technique (DSST), it is clear that, besides the aqueous chemistry, control of crystal morphology is essential in order to minimise membrane damage in the SPARRO process. In this process, there are three parameters that can be used control the morphology:

* Supersaturation to control nucleation
* Supersaturation to control growth
* Seed volume to control morphology

- If heterogeneous nucleation in the membrane is to be avoided, the supersaturation must be controlled. This can be manipulated by adjusting the water recovery.
- If sufficient seeds are provided, the morphology of the gypsum crystals can be controlled to the platelet shape, **even in regions where the needle morphology is dominant**. Thus, the membrane damaging needle-like morphology can be avoided.

Model design charts that relate seed volume and supersaturation or sulphate: calcium ratio to gypsum morphology in pure solutions have been developed.

10. RECOMMENDATIONS

From the membrane aspects of the work:

- Seeding with the platelet morphology could potentially minimise variations in membrane performance under typical operating conditions.
- Further experimentation using the SMTR mini-plant set up in order to obtain data for operating times in excess of 4000 hours, could provide the conclusive evidence required to confirm whether or not gypsum morphology, particularly of the needle type morphology, does have an influence on membrane damage. Consequently, should this be the case, the membrane damage is expected to be reduced by seeding with the platelet morphology.

The major recommendation arising from this work is related to the level of understanding of the chemistry of the mine waters being treated using the SPARRO process. It is clear that the quantitative information about the cations and anions present in the waters is often incomplete, which means that an understanding of the full extent of the aqueous chemistry interactions in the waters, as well as the future processing implications is not possible.

As a consequence, it is recommended that full analyses should always be carried out on waters of interest.

A second major recommendation arising from this work is related to the lack of understanding of the aqueous chemistry of complex mine waters. The preliminary modelling work carried out on the mine waters for this project has clearly shown that the complex chemistry arising from the interaction between cations and anions (and organic species - not covered in this work) has significant implications for both the type of scale formation expected as well as the degree of water recovery that is possible before scale formation becomes a problem.

As a consequence, it is recommended that future work focus on the aqueous chemistry of real mine waters, and the implications of that aqueous chemistry for interactions in the aqueous phase as well as for scaling species.

11. REFERENCES

Baldyga, J. and Bourne, J.R. (1989) Simplification of Micromixing Calculations. I. Derivation and Application of New Model. *The Chemical Engineering Journal*, **42**: 83-92.

Baldyga, J. and Bourne, J.R. (1999). *Turbulent Mixing and Chemical Reactions*. John Wiley and Sons, West Sussex.

Baldyga, J., Bourne, J.R. and Hearn, S.J. (1997) Interaction between chemical reactions and mixing on various scales. *Chemical Engineering Science*, **52**: 457-466.

Brandse, W.P., Van Rosmalen, G.M. and Brouwer, G. (1977). The influence of sodium chloride on the crystallisation rate of gypsum. *Journal of Inorganic and Nuclear Chemistry*, **39**: 2007-2010.

Bremere, I., Kennedy, M., Michel, P., van Emmerik, R., Witkamp, G. and Schippers, J. (1999) Controlling scaling in membrane filtration systems using a desalination unit. *Desalination*, **124**: 51-62.

Busby, R.W., Juby G.J.G., Pulles, W., and Nel, S., 1991. The evaluation of slurry reverse osmosis for the desalination of calcium sulphate scaling mine service water. Report to the Water Research Commission by the Chamber of Mines Research Organisation.

Çetin, E., Eroglu, I. and Ozkar, S. (2001) Kinetics of gypsum formation and growth during the dissolution of colemanite in sulfuric acid. Journal of Crystal Growth, 231: 559-567

Chen, J., Zheng, C. and Chen, G. (1996) Interaction of macro- and micromixing on particle size distribution in reactive precipitation. Chemical Engineering Science, 51: 1957-1966

Christoffersen, M.R., Christoffersen, J., Rosmalen, G.M., Weijnen, M.P.C. (1982), "Crystal growth of calcium sulphate dihydrate at low supersaturation", J. Crystal Growth, **58**, 585-595.

Doran, P. M. (1995). *Bioprocess engineering principles*. London: Academic Press

Franke, J. and Mersmann, A. (1995) The influence of the operational conditions on the precipitation process. *Chemical Engineering Science*, **50**: 1737-1753.

Gosele, W. & Kind, M. 1991, 'Study on the influence of mixing on the quality of continuous precipitating products', *Chem. Ing. Tech.*, vol. 63, pp. 59-61.

Gosele, W. and Kind, M. (1991) Study on the influence of mixing on the quality of continues precipitating products. *Chemie Ingenieur Technik*, **63**: 59-61.

Harnby, M. and Nienow, A. W. (1992). *Mixing in the process industries*. Oxford: Butterworth-Heinemann.

Harries, R.C., 1985. A field trial of seeded reverse osmosis for the desalination of a scaling-type mine water. Desalination. 56, 227-236.

INAP: International Network for Acid Prevention - Lorax Environmental October 2003, *Treatment of Sulphate in Mine Waters*,.

Juby, G.J.G, and Schutte C.F., 2000. Membrane life in a seeded slurry reverse osmosis system. Water SA, Vol 26, No. 2, April 2000.

Juby, G.J.G. (1994), "Development of a novel membrane desalination technique for treating calcium sulphate scaling mine water: the SPARRO process", PhD., University of Pretoria, South Africa.

Juby, G.J.G., Nel, D.J.C. and van der Merwe, I.W., 1998. Application of seeded reverse osmosis in South Africa for the recovery of water from $CaSO_4$ scaling water. WISA 98, Biennial conference and exhibition of the Water Institute of South Africa, May 1998, Cape Town, South Africa.

Juby, G.J.G., Pulles, W., Busby, R.W. (1992), "Development of the Slurry Precipitation and Recycle Reverse Osmosis (SPARRO) Technology For Desalinating Scaling Mine Waters", Wat. Sci. Tech. **25**, No. 10 pp 177-192.

Kramer H.J.M., Jansens P.J., 2002, Tools for designing and control of industrial crystallisers. In: Chianese, A. (eds) Proceedings of 15th International Symposium on Industrial Crystallisation, 15-18 September2002, Sorrento, Italy, pp 1089 – 1103

Lash, J.E. and Burns, G. (1984) Heats of crystallization of $CaSO_4.2H2O$. *Bulletin des Societes Chimiques Belges*, **93**: 271-279.

Lewis, A., Nathoo, J., Seewoo, S. and Lacour, S. (2002) "Prevention of scaling in mine waters using slurry precipitation and recycle reverse osmosis (SPARRO)", 15th International Symposium on Industrial Crystallisation, Sorrento (Italy).

Liu, S. and Nancollas, G.H. (1970) The kinetics of crystal growth of calcium sulfate dihydrate. *Journal of Crystal Growth*, **6**: 281-289.

Liu, S. and Nancollas, G.H. (1973) Linear crystallization and induction-period studies of the growth of calcium sulphate dihydrate crystals. *Talanta*, **20**: 211-216.

Liu, S. and Nancollas, G.H. (1975) A kinetic and morphological study of the seeded growth of calcium sulfate dihudrate in the presence of additives. *Journal of Colloid and Interface Science*, **52**: 593-601.

Loos, D., Pasel, C., Luckas, M., Schmidt, K. & Herbell, J. 2004, 'Experimental investigation and modelling of the solubility of calcite and gypsum in aqueous systems at higher ionic strenghth', *Fluid Phase Equilibria*, vol. 129, no. 2, pp. 219-229.

Mackay, J.G., Weichers, H.N.S., Pulles, W., Howarth, D., Busby, R.W., Combrink, C. (1991), Water quality and associated cost implications for the South African gold mining industry. Proc. 2nd Biennn. Conf. WISA. Johannesburg.

Maree, J.P., Greben, H.A. & de Beer, M. 2004, 'Treatment of acid and sulphate-rich effluents in an integrated biological/chemical process', *Water SA*, vol. 30, no. 2, pp. 183-190.

Miers, H.A. (1929). *An introduction to the scientific study of minerals.* Macmillan, London.

Mullin, J.W. (2001). *Crystallization.* Butterworth-Heinemann, Boston.

Nagata, S. (1975). *Mixing: principles and applications.* Tokyo: Kodansha New York.

Nesse, W. (2000). *Introduction to Minerology.* Oxford University Press, Oxford.

O'Hern, H.A., Rush F.E. (1963) Effect of mixing conditions in barium sulfate precipitation. *I & EC Fundamentals*, **2**:267-272.

Oldshue, J. Y. (1983). *Fluid mixing technology.* New York, N. Y: Chemical Engineering.

Othmer, K. (1995). *Encyclopedia of Chemical Technology.* John Wiley and Sons, New York.

Pohorecki, R., Baldyga, J. (1988) The effects of micromixing and the manner of reactor feeding on precipitation in stirred tank reactors, Chem.Eng.Sci.,1988, 43, 1949 -1954.

Roelands, C.P.M., Derksen, J.H., Kramer H J M.; Jansens, and Jansens, P.J. (2003) Analysis of mixing in a typical experimental set-up to measure nucleation rates of precipitation processes. *Chemical Engineering and Technology*, **26**: 296-303.

Seewoo, S., 2003. Morphology control in gypsum precipitation, MSc Thesis, University of Cape Town

Sheikholeslami, R. 2003, 'Mixed salts - scaling', *Desalination*, vol. 154, no. 2,15 April, pp. 117-127.

Sheikholeslami, R. 2004, 'Assessment of the scaling potential for sparingly soluble salts in RO and NF units', *Desalination*, vol. 167, no. 15 August, pp. 247-256.

Sluys, J.T.M., Bakkenes, H.W., van Marwijk, W.G., van Tongeren, W.G.J.M. and Hanemaaijer, J.H., 2001. MmmYMAAS masters metals, TNO publication.

Sohnel, O. and Garside, J. (1992). *Precipitation.* Butterworth-Heinemann Ltd, Oxford.

Torbacke, M. and Rasmuson, A.C. (2001) Influence of different scales of mixing in reaction crystallisation. *Chemical Engineering Science.*, **56**: 2459-2473.

Uhl, V.W. and Gray, J.B. (1966). *Mixing.* Academic Press, New York.

Verdoes D., and Hanemaaijer, J.H.,1994, Method and appliance for removing at least one constituent from solution, European Patent EP 0669898

Verdoes, D. and Hanemaaijer, J.H. (1996). Membrane-assisted crystallization: a new hybrid process exemplified by the softening of water. In J. Ulrich and K. Wangnick (Ed.), *Bremen International Workshop on Industrial Crystallization* (pp. 92-99).

Willey, J.D. 2004, 'The Effect of Ionic Strength on the Solubility of an Electrolyte', *Journal of Chemistry Education*, vol. 18, pp. 1644.

Wong, D.C.Y., Jaworski, Z. and Nienow, A.W. (2001) Effect of ion excess on particle size and morphology during barium sulphate precipitation: an experimental study. *Chemical Engineering Science*, **56**, 727-734.

Yu, H., Sheikholeslami, R. & Doherty, W.O.S. 2002, 'Mechanisms, thermodynamics and kinetics of composite fouling of calcium oxalte and amorphous silica in sugar mill evaporators - A preliminary study', *Chemical Engineering Science*, vol. 57, no. 11, pp. 1969-1978.

TO ORDER: Contact **Publications** - Telephone No: 012 330 0340
Fax Number: 012 331 2565
E-mail: publications@wrc.org.za

Water Research Commission
Private Bag X03, Gezina, 0031, South Africa
Tel: +27 12 330 0340, Fax: +27 12 331 2565
Web: http://www.wrc.org.za